2015

Quality Factor of Horizontal Wire Dipole Antennas near Planar Conductor or Dielectric Interface

Adebayo Gabriel Adeyemi
University of Massachusetts Amherst

QUALITY FACTOR OF HORIZONTAL WIRE DIPOLE ANTENNAS NEAR PLANAR CONDUCTOR OR DIELECTRIC INTERFACE

A Thesis Presented

by

ADEBAYO ADEYEMI

Submitted to the Graduate School of the
University of Massachusetts Amherst in partial fulfillment
of the requirements for the degree of

MASTER OF SCIENCE IN ELECTRICAL AND COMPUTER ENGINEERING

February 2015

Electrical and Computer Engineering

QUALITY FACTOR OF HORIZONTAL WIRE DIPOLE ANTENNAS NEAR PLANAR CONDUCTOR OR DIELECTRIC INTERFACE

A Thesis Presented

by

ADEBAYO ADEYEMI

Approved as to style and content by:

Do-Hoon Kwon, Chair

Ramakrishna Janaswamy, Member

Robert W. Jackson, Member

Christopher V. Hollot, Department Chair
Electrical and Computer Engineering

To my parents.

ACKNOWLEDGMENTS

I would like to dedicate this thesis to my parents, fiance, and the Adedirans'. I also want to say thank you to all professors in ECE department especially Professor Do-Hoon Kwon for all didactic ability he used during this work. To all my friends in the CASCA lab namely; Hua Bai , Yutong Yang, Hseih-Chi Chang, Caglar Emiroglu, Amin Nikravan, and others, I am grateful for all your support during this work. My final gratitude goes to God.

ABSTRACT

QUALITY FACTOR OF HORIZONTAL WIRE DIPOLE ANTENNAS NEAR PLANAR CONDUCTOR OR DIELECTRIC INTERFACE

FEBRUARY 2015

ADEBAYO ADEYEMI

B.Sc., UNIVERSITY OF MASSACHUSETTS, AMHERST

M.S.E.C.E., UNIVERSITY OF MASSACHUSETTS AMHERST

Directed by: Professor Do-Hoon Kwon

Quality factor of a dipole over a conducting ground plane is predicted. Quality factor is also generated as a function of the electrical ground separation and the electrical length. The optimal ground separation for largest bandwidth is obtained. A dipole near a dielectric interface is also studied for quality factor prediction. The predicted quality factor is generated as a function of position and electrical length. Quality factor is generated for a dipole inside the dielectric half space, and a dipole above the dielectric half space.

TABLE OF CONTENTS

LIST OF TABLES

Table **Page**

LIST OF FIGURES

Figure **Page**

CHAPTER 1

INTRODUCTION

Fundamental limits on small antennas have been an interesting topic of research since 1947. Chu [1] and McLean[2], for example, found physical limits on small antennas in terms of the radiation quality factor Q. Quality factor is an important performance parameter in describing the transmission and receiving capability of an antenna because it is related to gain, beam-width, impedance and radiation pattern. For antennas in free space, physical limits on linearly polarized antenna has been illustrated [3]. In [3], Gutstafson *et al.* describe a physical limit on antennas as

$$G_K(\hat{\boldsymbol{k}}, \hat{\boldsymbol{e}})B \leq \frac{2\eta(-\hat{\boldsymbol{k}}, \hat{\boldsymbol{e}})k_c^3}{2}\left(\hat{\boldsymbol{e}} \cdot \boldsymbol{\gamma}_\infty \cdot \hat{\boldsymbol{e}} + (\hat{\boldsymbol{k}} \times \hat{\boldsymbol{e}}) \cdot \boldsymbol{\gamma}_\infty \cdot (\hat{\boldsymbol{k}} \times \hat{\boldsymbol{e}})\right). \tag{1.1}$$

where G_K is the minimum partial realized gain, $\hat{\boldsymbol{k}}$ is the direction of the incident wave, $\hat{\boldsymbol{e}}$ is the preferred polarization, k_c is the first dominant resonance wavenumber, B is the fractional bandwidth, η is the absorption efficiency that is closely approximated by 0.5, and $\boldsymbol{\gamma}_\infty$ is the high-contrast polarizability dyadics.

However, practical antennas do not operate in free space, but in realistic environments. For example, an antenna may operate in the presence of a large ground plane or a conducting platform. A penetrable scatterer may be present in the vicinity. This makes the bandwidth limit of a conductor- or material-backed antenna an interesting topic of practical importance. In the presence of a ground plane or a material half space, the quality factor Q is an equally applicable descriptor of bandwidth for narrowband resonant antennas.

In this study , an approximate quality factor Q of a dipole over a ground plane in terms of ground separation is obtained. In addition, the Q of a wire dipole in the presence of a lossless dielectric half space is studied. For a thin-wire dipole, the Q is found in terms of the electrical separation between the wire dipole and the half space, and the electrical length of the dipole. Both cases of the dipole on the free space side and in the dielectric half space are considered. The effect of the permittivity of the dielectric half space is analyzed by investigating Q in terms of the relative permittivity for a dipole of fixed electrical length and position from the free space dielectric interface.

This thesis is arranged as follows; An overview of limitations of free space antennas in terms of a quality factor is provided in Chapter 2. Chapter 3 investigates the Q bound of a dipole backed by a conducting ground plane. A dipole will be placed at different heights from the PEC ground and the height that is associated with the smallest quality factor(largest bandwidth) will be noted. The Q bound is based on an approximate integral identity for the extinction cross section of a conductor backed dipole. A closed form expression will be derived for the dipole. In Chapter 4, the quality factor of a dipole backed by dielectric half space will be discussed. A numerical method is used to obtain the Q lower bound. Finally, in Chapter 5, the quality factor of a dipole immersed in a dielectric half space will be discussed.

CHAPTER 2

BANDWIDTH LIMITATION OF SMALL ANTENNAS IN FREE SPACE

The radiation quality factor (Q_{rad}) of electrically small antennas has been an interesting part of research in antenna community for decades. The most cited work on the quality factor of electrically small antenna is Chu's radiation Q for omnidirectional antennas. In 1948, he found a lower bound on Q_{rad} using a sphere enclosing an electrically small antenna by exciting only the lowest TM spherical mode to account for the external field enclosing the antenna [1]. A dipole antenna of length $l \approx 2a$ is enclosed by a sphere of radius a as shown in Figure 2.1.

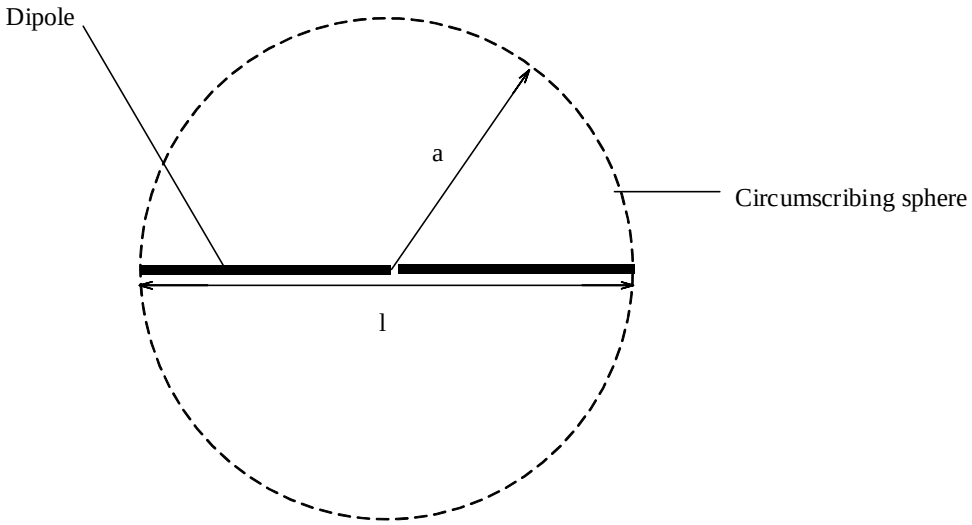

Figure 2.1. A dipole antenna enclosed by a sphere.

The lower limit is

$$Q_{rad} = \frac{1}{ka} + \frac{1}{k^3 a^3}. \tag{2.1}$$

For quality factor limit on small antennas, however, Chu was not the first to consider this limit. Prior to Chu's work, Wheeler [4] already noted that the frequency bandwidth limitation for narrow band antennas depend on their sizes with effects on radiation pattern and invariably the practical efficiency of the antenna. Later on, Collin and Rothschild [5] expanded Chu's work to cylindrical geometries. In 1969, Fante [6] took a new path on the problem by deriving an expression for Q by incorporating both TM and TE excitation mode, unlike only TM excitation modes in Chu's bandwidth limit. Another drawback of Chu's lower bound is that the energy stored inside the hypothetical circumscribing sphere was not included.This makes the Chu bound a conservative limit, which may not be easily approached using realistic antennas. For spherical antennas, Thal [7] gave an exact calculation that includes the energy stored inside as well as outside the sphere. However, the Thal bound on Q was given in terms of numerical values. Collins and Hansen[8] gave an approximate, simplified formula for Thal bound as

$$Q \approx \frac{1}{\sqrt{2}ka} + \frac{3}{2(ka)^3}. \tag{2.2}$$

Recently, Gustafsson *et al*. [3] studied the effect of antenna's shape on bandwidth. Gustafsson's physical limitation on antennas is closely related to this thesis because the same technique was used to derive the Q bound for narrowband antennas. This technique is discussed in Section 2.1.

Most of the work on the quality factor Q of electrically small antennas is applicable to antennas in free space. However, practical antennas do not operate in free space. Often they are in the vicinity of a conductor or a material. Therefore, understanding the quality factor of an antenna when it is placed in the vicinity of a conductor or a material is important. The radiation Q of an electrically small antenna close to a conducting plane has been studied by Sten *et al* [9]. They used a single large sphere that encloses the small antenna and its image. Then, the Chu lower bound expression

was used on this sphere. The resulting Q turns out to be too conservative (too low to be approached by practical antennas). Chang *et al*. [10] obtained a tight lower bound on the radiation Q for electrical small antennas over a conducting ground plane by evaluating energies both internal and external to the spherical antenna surface in the presence of a ground plane. In all, bounds on the antenna Q that have been reported to date are mostly for small antennas of spherical shape. Although spherically shaped antennas are convenient for analysis using spherical vector wave functions, practical antennas are not of spherical shape.

In this thesis, therefore, the Q of an horizontal dipole placed near a conducting ground will be investigated. In addition, Q of an horizontal dipole near a dielectric half space will also be studied. Derivation of Q lower bounds in these scenarios are based on the technique used by Gustafsson *et al*. An brief explanation of the technique is provided in the following the Section 2.1.

2.1 Limitations of Antennas of Arbitrary Shapes Based on Scattering Technique

Due to the ease of analysis using spherical vector wave functions, the lower bounds on the radiation Q is typically given in terms of the dimension of the smallest sphere that encloses the antenna geometry [1] [4]. However, sphere is not usually a practical antenna geometry. Treating antennas as scatterers, its physical limitation can be found incorporating the effect of the antenna shape. Gustafsson *et al* derived physical limitations on bandwidth, quality factor, directivity and realized gain for antennas of arbitrary shape based on a scattering technique [11]. Also, the derived bandwidth bound clarifies the contribution of the magnetic and the electric properties of the antenna. Since this thesis is based on the same approach used by Gustafsson *et al*, this scattering-based technique is explained.

Antennas can be considered as scatterers as well as absorbers of electromagnetic waves.

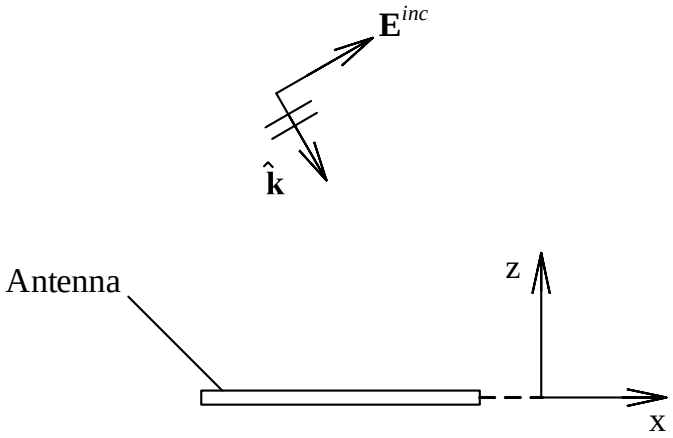

Figure 2.2. Antenna subject to plane wave illumination.

A linearly polarized plane wave, $\mathbf{E}^{inc} = \hat{\boldsymbol{e}} E_0 e^{-jk\hat{\boldsymbol{k}}\cdot\boldsymbol{r}}$, incident on an antenna is scattered and absorbed by the antenna as illustrated in Figure 2.2. A complex function h in terms of the scattering dyadic $\mathbf{S}$ is defined as [11]

$$h(k;\hat{\boldsymbol{k}},\hat{\mathbf{e}}) = 4\pi \frac{\hat{\mathbf{e}}\cdot\mathbf{S}(k;\hat{\boldsymbol{k}})\cdot\hat{\mathbf{e}}}{k}. \tag{2.3}$$

where $\hat{\mathbf{e}}$ is the electric polarization of the incident wave, $\hat{\boldsymbol{k}}$ is the incident direction, k is the free space wavenumber, and $\mathbf{S}$ is the scattering dyadic. Then, h is an analytic function in the lower half of the complex-k plane [11] in Figure 2.3, which is $\mathrm{Im}\{k\} < 0$. The function h is related to the extinction cross section, $\sigma_{ext}(k;\hat{\boldsymbol{k}},\hat{\mathbf{e}})$, through the optical theorem as $\mathrm{Im}\, h(k;\hat{\boldsymbol{k}},\hat{\mathbf{e}}) = \sigma_{ext}(k;\hat{\boldsymbol{k}},\hat{\mathbf{e}})$. The low frequency behavior of h is given by [12]

$$h(k;\hat{\boldsymbol{k}},\hat{\mathbf{e}}) = \Big(\hat{\boldsymbol{e}}\cdot\boldsymbol{\gamma}_e\cdot\hat{\boldsymbol{e}} + (\hat{\boldsymbol{k}}\times\hat{\boldsymbol{e}})\cdot\boldsymbol{\gamma}_m\cdot(\hat{\boldsymbol{k}}\times\hat{\boldsymbol{e}})\Big)\, k + \mathcal{O}(k^2) \qquad as\ k\to 0. \tag{2.4}$$

where $\boldsymbol{\gamma}_e$ and $\boldsymbol{\gamma}_m$ are the electrostatic and magnetostatic polarizability dyadic respectively.

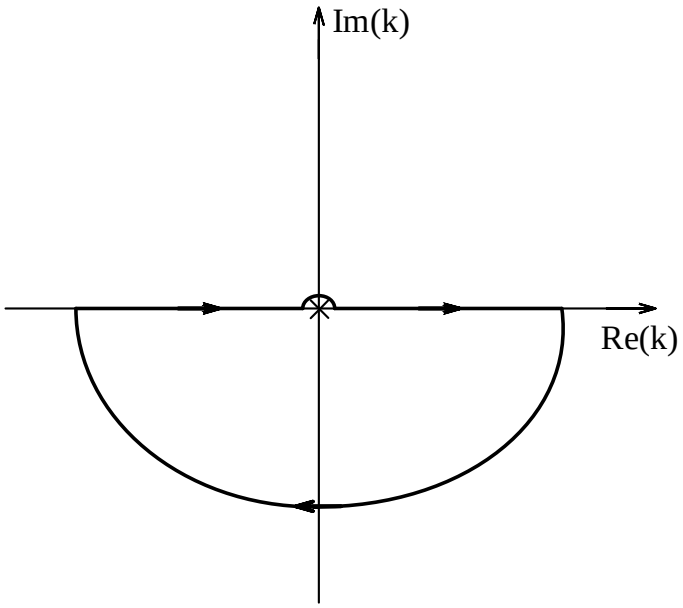

Figure 2.3. Integration contour in the complex k-plane.

This leads to integral for the extinction cross section and the resulting sum rule is [11]

$$\int_0^\infty \frac{\sigma_{ext}(k)}{k^2} dk = \frac{\pi}{2} \left(\hat{\boldsymbol{e}} \cdot \boldsymbol{\gamma}_e \cdot \hat{\boldsymbol{e}} + (\hat{\boldsymbol{k}} \times \hat{\boldsymbol{e}}) \cdot \boldsymbol{\gamma}_m \cdot (\hat{\boldsymbol{k}} \times \hat{\boldsymbol{e}}) \right) \tag{2.5}$$

where σ_{ext} is the sum of the absorption and the scattering cross sections of the antenna under a plane wave illumination. It is noted that σ_{ext} is non-negative and real valued. The left hand side of (2.5) is frequency dependent, and the right hand side of (2.5) depends on the material property and shape of the antenna at zero frequency. This sum rule is applicable to antennas of arbitrary shape where the effect of the shape is incorporated in the polarizability values.

A physical bound on the ratio of directivity and Q for an electrically small antenna in free space is achieved, and Gustafsson's D/Q limit for an antenna in free space [11] is

$$\frac{D}{Q} \leq \frac{\eta k_c^3}{2\pi} \left(\hat{\boldsymbol{e}} \cdot \boldsymbol{\gamma}_\infty \cdot \hat{\boldsymbol{e}} + (\hat{\boldsymbol{k}} \times \hat{\boldsymbol{e}}) \cdot \boldsymbol{\gamma}_\infty \cdot (\hat{\boldsymbol{k}} \times \hat{\boldsymbol{e}}) \right). \tag{2.6}$$

where $\hat{\boldsymbol{k}}$ is the direction of the incident wave, $\hat{\boldsymbol{e}}$ is the preferred polarization, D is the directivity, Q is the quality factor, k_c is the first dominant resonant wavenumber, η is the absorption efficiency that is closely approximated by 0.5, and $\boldsymbol{\gamma}_\infty$ is the high-contrast polarizability dyadics. Since D of small antennas is approximately 1.5, Q for a small antenna can be obtained from (2.6).

CHAPTER 3

DIPOLE BACKED BY A CONDUCTING GROUND PLANE

3.1 Approximate Integral Identity for a Wire Dipole over a Ground Plane

A cylindrical thin-wire dipole of radius a and length l that is placed above an infinite perfect electric conductor(PEC) ground plane at the distance d is subject to a linearly polarized plane wave illumination as shown in Figure 3.1 and it is denoted as problem a. For the purpose of expressing the extinction cross section, a free space

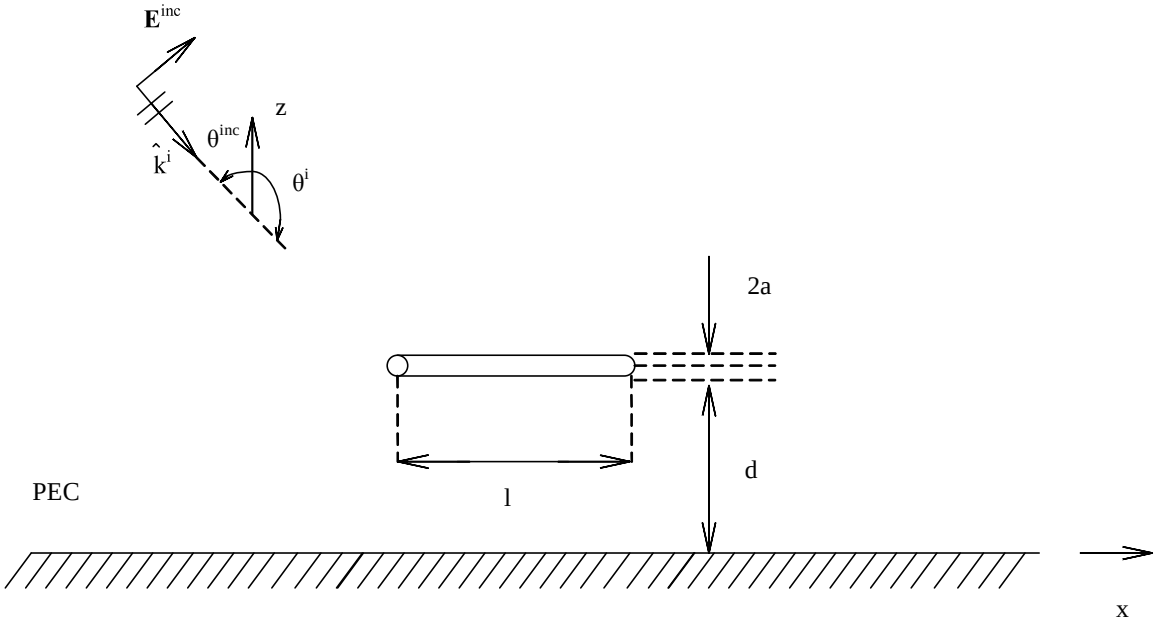

Figure 3.1. A dipole above a PEC ground(problem a).

configuration having two antennas and one incident plane wave is defined as shown in Figure 3.2 and it is denoted as problem b.

The PEC ground is removed and an image dipole is placed at the image position of the original dipole. These two dipoles in free space are now separated by $2d$. Note that problem b is not a result of the image theory because no image of the incident field is present. This is now a problem of two antenna in free space under plane wave

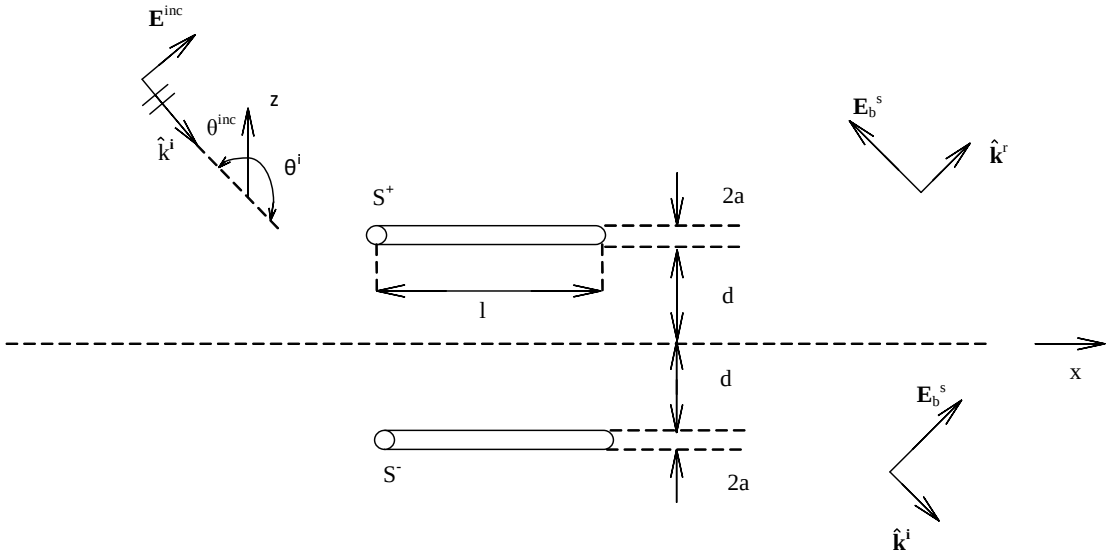

Figure 3.2. Free space configuration for a dipole above a PEC ground(problem b).

illumination. The extinction cross section of the dipole over a ground plane of interest (problem a) is expressed as

$$\sigma_{ext} = -\frac{4\pi}{k}\mathrm{Im}\left\{\hat{e}^{r*}\cdot\mathbf{S}_a\left(k,\hat{k}^r\right)\cdot\hat{e}^i\right\}, \tag{3.1}$$

which is the optical theorem for a scatterer over a PEC ground. It is given in terms of the complex amplitude of the scattering dyadic $\mathbf{S}_a$ in the direction of specular reflection and the wavenumber k. Since an integral identity for σ_{ext} is sought, the antenna is treated as a scatterer of a plane wave rather than a radiator. Often in the antenna community, a surface equivalent principle same as Huygens principle is employed when the radiation problem is replaced with scattering problem [13]. For scatterers in free space, the extinction cross section($\sigma_{ext}(k)$) is related to the forward

scattering coefficient of the far field of scatterer through the optical theorem. Rather than analyzing scattering in the presence of a ground plane, it is easier to treat scattering in free space. Problem b in Figure 3.2 describes scattering by two antennas in free space. Although problem b is not equivalent to problem a via the image theory, the extinction cross section of problem a is related to the free space scattering characteristics of problem b. In terms of the scattering coefficient of problem b in the forward and specular directions, $\sigma_{ext}(k)$ is expressed as

$$\sigma_{ext}(k) = -\frac{4\pi}{k}\mathrm{Im}\left\{\hat{e}^{r*}\cdot\mathbf{S}_b(k,\hat{k}^r)\cdot\hat{e}^i + \hat{e}^{i*}\cdot\mathbf{S}_b(k,\hat{k}^i)\cdot\hat{e}^i\right\}, \tag{3.2}$$

where $\mathbf{S}_b$ is the scattering amplitude dyadic, k is the free space wavenumber, $\hat{e}^r$ and $\hat{e}^i$ are the unit vectors of polarization of the specular field and the incident field respectively. The scattering amplitude dyadic is related to the far zone scattered field as

$$\mathbf{E}_b^s = \frac{e^{-jkr}}{r}\mathbf{S}_b\cdot\mathbf{E}^{inc}. \tag{3.3}$$

Position vector, polarization vector, and propagation vector can be decomposed into vertical and transverse component as $\mathbf{r}' = \mathbf{r}_t + \hat{z}z'$, $\hat{e}_i = \mathbf{e}_t + \hat{z}e_z$ and $k\hat{k}_i = \mathbf{k}_t + \hat{z}k_z$ respectively. σ_{ext} can be written in terms of total fields in problem b as

$$\begin{aligned}\sigma_{ext}(k) = \frac{1}{|E_0|}\mathrm{Im}\{-2\mathbf{e}_t^*\cdot\oint_S \mathbf{r}'\hat{n}\cdot[(\mathbf{k}_t j\sin k_z z' + \hat{z}k_z\cos k_z z')\times\eta_0\mathbf{H}_b \\ + jk\sin k_z z'\mathbf{E}_b]e^{j\mathbf{k}_t\cdot\mathbf{r}_t'}ds' + \hat{z}j2\mathbf{e}_z^*\cdot\oint_S \mathbf{r}'\hat{n}\cdot[(\mathbf{k}_t j\cos k_z z' \\ -\hat{z}k_z\sin k_z z')\times\eta_0\mathbf{H}_b + jk\cos k_z z'\mathbf{E}_b]e^{j\mathbf{k}_t\cdot\mathbf{r}_t'}ds'\},\end{aligned} \tag{3.4}$$

where η_0 is the free space impedance and S contains both S^+ and S^-. Magnetic surface current terms for problem b are not in (3.4) because the thin-wire dipole is

perfectly conducting. Now the electric field $\mathbf{E}_b$ over S^+ and S^- is asymptotically at low frequency and it can be written as [14]

$$\mathbf{E}_b(\mathbf{r}') = \mathbf{E}_{b0}(\mathbf{r}')e^{-jk\hat{k}^i\cdot\mathbf{r}'}, \qquad k \to 0, \tag{3.5}$$

where $\mathbf{E}_{b0}(\mathbf{r}')$ is the static electric field distribution. In the low frequency limit ($k \to 0$), it can be shown that $\sigma_{ext}(k)$ is expressed as [14]

$$\sigma_{ext}(k) = \mathrm{Im}\left\{4k[(\boldsymbol{e}_t^* \cdot \boldsymbol{\gamma}_{be} \cdot \hat{e}^i)\sin^2 k_z d + (\hat{z}\boldsymbol{e}_z^* \cdot \boldsymbol{\gamma}_{be} \cdot \hat{e}^i)\cos^2 k_z d]\right\}, \qquad k \to 0, \tag{3.6}$$

Where $\boldsymbol{\gamma}_{be}$ is the electric polarizability of one antenna of the two antennas in problem b, $\boldsymbol{e}_z^*$ is the z-component vector of the polarization unit vector and $\boldsymbol{e}_t^*$ is the remaining portion of the polarization unit vector contained in the xy-plane. For horizontal thin-wire dipole, the induced dipole moment has no z-component for a dipole illuminated with normal incident plane wave. Therefore, the second term in the bracket in (3.6) is equal to zero. Dividing both sides of (3.6) by $k^2\sin^2(kd\cos\theta^i)$ and applying Cauchy integral theorem by integrating over a closed contour in the lower half of the complex plane [3], we obtain

$$\int_0^\infty \frac{\sigma_{ext}(k)}{k^2\sin^2(kd\cos\theta^i)}dk = 2\pi\boldsymbol{e}_t^* \cdot \boldsymbol{\gamma}_{be} \cdot \hat{e}^i. \tag{3.7}$$

This relates the extinction cross section of the antenna to its static electric polarizability via a weighted extinction cross section integrated over all positive real frequency. The agreement between the rhs and lhs of (3.7) is listed in Table 3.1. Except at the smallest separation, a reasonable agreement is observed between the two sides.

To establish the approximate nature of the sum rule (3.7), consider the extinction

Table 3.1. Validation of the integral identity for a wire dipole above a PEC ground.

Separation(d)	LHS	COMSOL($\mathbf{p}$)	RHS	Percent diff.
1.00	7.50e-3	1.17e-3	7.35e-3	1.3
0.50	7.50e-3	1.17e-3	7.35e-3	1.3
0.45	7.50e-3	1.17e-3	7.35e-3	1.3
0.40	7.00e-3	1.17e-3	7.35e-3	5.4
0.35	7.00e-3	1.17e-3	7.35e-3	5.4
0.30	7.00e-3	1.17e-3	7.35e-3	5.4
0.25	7.00e-3	1.17e-3	7.35e-3	5.4
0.20	7.00e-3	1.17e-3	7.35e-3	5.4
0.15	6.80e-3	1.17e-3	7.35e-3	8.1
0.10	6.90e-3	1.16e-3	7.29e-3	6.8
0.05	7.00e-3	1.13e-3	7.10e-3	1.4
0.04	7.20e-3	1.11e-3	6.90e-3	4.1
0.03	7.50e-3	1.10e-3	6.90e-3	4.2
0.02	6.80e-3	1.01e-3	6.30e-3	7.4
0.01	6.80e-3	9.40e-4	5.70e-3	13.2

cross section $\sigma_{ext}(k)$ for problem b in Figure 3.2. It is given in terms of the scattering amplitude dyadic $\mathbf{S}_b$ as

$$\sigma_{b,ext}(k) = -\frac{4\pi}{k}\mathrm{Im}\left\{\hat{e}^{i*}\cdot\mathbf{S}_b\left(k,\hat{k}^i\right)\cdot\hat{e}^i\right\}. \tag{3.8}$$

Define the function $h_b = (-4\pi/k)\hat{e}^{i*}\cdot\mathbf{S}_b\left(k,\hat{k}^i\right)\cdot\hat{e}^i$ such that $\sigma_{b,ext}(k) = \mathrm{Im}\{h_b\}$. Limiting our attention to thin-wire antennas with the wire axis parallel to the xy-plane so that the magnetic polarizability is negligible, it follows that h_b is analytic in the low-half of the complex-k plane [11] and

$$h_b = \left[\hat{e}^{i*}\cdot(2\boldsymbol{\gamma}_{be})\cdot\hat{e}\right]k + \mathcal{O}\left(k^2\right), \qquad k\to 0, \tag{3.9}$$

where the factor of two accounts for the presence of two identical antennas. The integral sum rule for $\sigma_{b,ext}(k)$ is

$$\int_0^\infty \frac{\sigma_{b,ext}(k)}{k^2}dk = \frac{\pi}{2}\boldsymbol{e}_t^*\cdot(2\boldsymbol{\gamma}_{be})\cdot\hat{e}^i. \tag{3.10}$$

In (3.2), define $h_a = (-\frac{4\pi}{k}) \left\{ \hat{e}^{r*} \cdot \mathbf{S}_b(k, \hat{k}^r) \cdot \hat{e}^i + \hat{e}^{i*} \cdot \mathbf{S}_b(k, \hat{k}^i) \cdot \hat{e}^i \right\}$ such that $\sigma_{ext}(k) = \text{Im}\{h_a\}$. For thin-wire antennas under consideration, a PEC wire parallel with the xy-plane with the z-coordinate limited to $z = d$, we have

$$h_a = 2h_b \sin^2 k_z d. \tag{3.11}$$

Using (3.11) in the derivation of (3.10) leads to (3.7). The additional assumption used in writing (3.11) is $\mathbf{E}_b = \mathbf{E}_{b0} e^{-jk\hat{k}^i \cdot \mathbf{r}'}$, where $\mathbf{E}_{b0}$ represents the amplitude of the surface field on the two antennas that possesses a mirror symmetry with respect to the xy-plane. This condition assumes that the boundary electric field of one antenna is not affected by the presence of the other antenna. In other words, the boundary field of either antenna in problem b is the same as when the other antenna is absent. This assumption is expected to be accurate when the ground separation d is large. Hence, the approximate sum rule (3.7) is expected to be accurate for wire antennas that are not too close to the ground plane.

A polarizability represents the physical property of the scatterer. It is a measure of responsiveness of a local element to the external field, and it is defined in terms of the induced dipole moment of the particle. The polarizability of a scatterer(an antenna in our case) depends on the shape and material of the object. In statics, there are electrostatic and magnetostatic polarizabilities. In our case, the electrostatic polarizability, $\boldsymbol{\gamma}_{be}$, of a perfectly conducting thin circular cylinder is relevant. The polarizability value will be obtained numerically in this thesis for a typical wire dipole. The focus will be obtaining a physical bound on the bandwidth of the antenna in terms of the resonance quality factor, Q, and in terms of the electrostatic polarizability. A discussion on evaluation of polarizability from COMSOL is in appendix B.

3.2 Lower Bound of the Resonance Quality Factor (Q)

Starting from the integral identity (3.7), it is desired to find a lower bound for the resonance quality factor Q. The extinction cross section $\sigma_{ext}(k)$ is related to the scattering cross section of an antenna and the absorption cross section of the antenna. It is the sum of the two cross sections, i.e, $\sigma_{ext}(k) = \sigma_s(k) + \sigma_a(k)$ where $\sigma_s(k)$ is the scattering cross section and $\sigma_a(k)$ is the absorption cross section. For a lossless antenna under plane wave illumination, the absorbed power corresponds to the power received and delivered to the load. Since cross sections are non-negative real quantities, we have

$$\sigma_{ext}(k) \geq \sigma_a(k). \tag{3.12}$$

This inequality can be used to derive the bandwidth bound of the antenna. However, the equality in (3.12) means that there is no scattering at all, which is not possible for a recieving antenna.. Therefore, bandwidth bounds derived from (3.14) tend to be too conservative. By introducing an absorption efficiency, a tight bandwidth bound may be obtained. Hence, we use

$$\sigma_{ext}(k) \approx \sigma_a(k)/\eta_{abs}. \tag{3.13}$$

where η_{abs} is the absorption efficiency. For narrowband antennas around the resonance frequency where impedance is matched, it is known that η_{abs} is approximately equal to 0.5 [3]. (3.13) will be used to find the lower bound on the quality factor. In antenna terms, the absorption cross section can also be written as

$$\sigma_a(k) = A_{em}(k)(1 - |\Gamma(k)|^2), \tag{3.14}$$

where $A_{em}(k)$ is the maximum effective area of the antenna [13], and $(1 - |\Gamma(k)|^2)$ is the impedance mismatch factor or reflection effeciency. Now $\sigma_{ext}(k)$ can be replaced

in (3.7) to give

$$\frac{1}{\eta_{abs}} \int_0^\infty \frac{A_{em}(k)(1-|\Gamma(k)|^2)}{k^2 \sin^2(kd\cos\theta^i)} dk \approx 2\pi \boldsymbol{e}_t^* \cdot \boldsymbol{\gamma}_{be} \cdot \hat{e}^i. \tag{3.15}$$

Since $A_{em}(k)$ can also be written in terms of the directivity D as $\frac{\lambda^2 D}{4\pi}$. (3.15) can then be written as

$$\frac{\pi}{\eta_{abs}} \int_0^\infty \frac{D(k)(1-|\Gamma(k)|^2)}{k^4 \sin^2(kd\cos\theta^i)} dk \approx 2\pi \boldsymbol{e}_t^* \cdot \boldsymbol{\gamma}_{be} \cdot \hat{e}^i, \tag{3.16}$$

where $\lambda = \frac{2\pi}{k}$ has been used. Also, the constant factors can be pulled out of the integral in (3.15). For the study of a thin-wire dipole backed by a PEC ground plane, let us choose a normally incident plane wave (θ^i=0). The directivity in the direction of the incoming wave and the mismatch $1-|\Gamma(k)|^2$ both depend on the wavenumber k, so, they have to remain inside the integral. At this point, the frequency dependent $D(k)$ and $1-|\Gamma(k)|^2$ may be replaced by mathematical models appropriate for resonant antennas. The models are discussed in the following subsections.

3.2.1 Model for $D(k)$

The directivity of an horizontal infinitesimal dipole over a PEC ground plane is available in [13], which is equal to

$$D(k) = \frac{4\sin^2(kd)}{R(kd)}, \tag{3.17}$$

where d is the distance from the dipole to the ground plane. The function $R(kd)$ is a factor that appears in the radiated power expression and it is given by

$$R(kd) = \left[\frac{2}{3} - \frac{\sin(2kd)}{2kd} - \frac{\cos(2kd)}{(2kd)^2} + \frac{\sin(2kd)}{(2kd)^3}\right]. \tag{3.18}$$

The expression for directivity, in (3.17), for an infinitesimal dipole used to derive a Q bound is not a function of the antenna size. Since the Q bound derived from (3.16) depends on the directivity as a function of frequency, it will be accurate for small antennas and the accuracy will degrade for larger antennas. The Q bound will be tested using a self-resonant dipole of approximately a half-wavelength. Therefore, it is important to recognize the difference between the directivities of infinitesimal and short(up to a half wavelength) dipoles. In Figure 3.3, directivity in the +z axis direction is compared with respect to frequency between an infinitesimal dipole and a thin-wire dipole of length $l = 0.2$m obtained using the numerical analysis package FEKO based on method of moments technique. The directivity model is compared with the simulated directivity in the low frequency range, where the physical antenna may be approximated as an infinitesimally short antenna as shown in Figure 3.3. With increasing frequency, the physical antenna has a higher directivity than the infinitesimally short dipole over the range of ground separation less than a half wavelength.

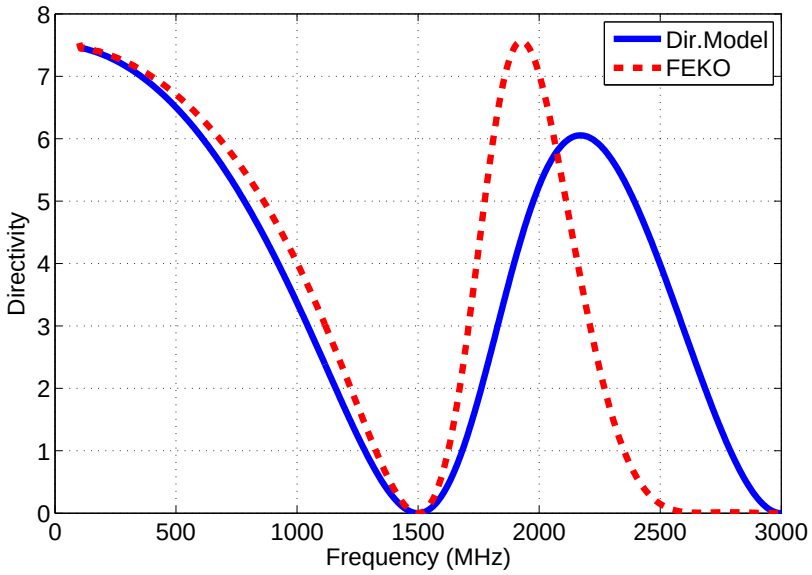

Figure 3.3. Comparing directivity from FEKO and model at $d = 0.25$ m.

3.2.2 Model for $1 - |\Gamma(k)|^2$

Similar to a thin wire dipole antenna in free space, a conductor-backed dipole will be a resonant antenna that operates over a narrow bandwidth. A typical resonant response for the reflection coefficient is illustrated in Figure 3.4,

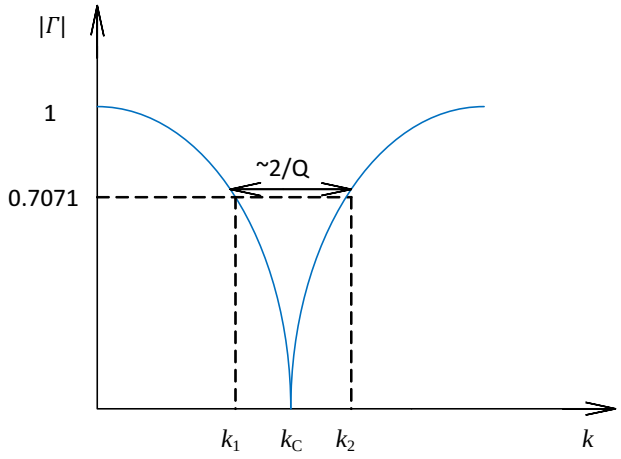

Figure 3.4. Single narrow band model.

and the associated mismatch factor is shown in Figure 3.5. Around the resonance frequency f_c, the resonant behavior of the narrowband antenna may be represented by the response of a second-order resonant circuit. Considering a series-RLC circuit, a quality factor Q can be associated with the circuit response around resonance. The mismatch factor $1 - |\Gamma(k)|^2$ of a series resonance circuit can be written as [15]

$$1 - |\Gamma(k)|^2 = \frac{1}{1 + (\frac{Q}{2})^2(\frac{k}{k_c} - \frac{k_c}{k})^2}, \tag{3.19}$$

where k_c is the wavenumber at resonance and it is noted that $1-|\Gamma(k)|^2 = \mathcal{O}(k^2)$ as $k \to 0$. Use of parallel-RLC circuit leads to the same expression for the mismatch factor. The wavenumbers k_1 and k_2 denote the edge wavelengths referenced to the half-power points on both sides of k_c, which are related to k_c via $k_c = \sqrt{k_1 k_2}$. The quality factor Q of this resonance is related to the 3dB fractional bandwidth via

$$\frac{2}{Q} = \frac{k_2 - k_1}{k_c}. \tag{3.20}$$

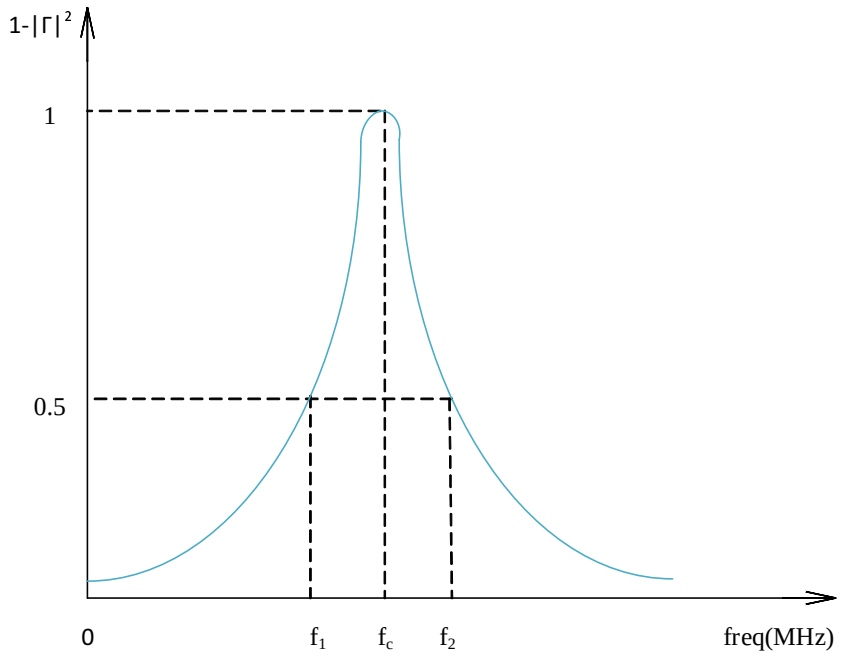

Figure 3.5. Narrow band mismatch $1 - |\Gamma(k)|^2$ model.

For a dipole over a ground plane, it was observed from simulated results in Figure 3.7 that $1-|\Gamma(k)|^2 = \mathcal{O}(k^4)$ as $k \to 0$. A proper model for $1-|\Gamma|^2$ should not only be accurate around the resonance wavelength, but also should have a correct order of k at low frequencies. Hence, the mathematical model for impedance mismatch factor for a dipole over a PEC ground plane is defined as

$$1 - |\Gamma(k)|^2 = \frac{k^2 R(kd)}{k_c^2 R(k_c d)(1 + (\frac{Q}{2})^2(\frac{k}{k_c} - \frac{k_c}{k})^2)}, \tag{3.21}$$

where

$$R(k_c d) = \left[\frac{2}{3} - \frac{\sin(2k_c d)}{2k_c d} - \frac{\cos(2k_c d)}{(2k_c d)^2} + \frac{\sin(2k_c d)}{(2k_c d)^3}\right] \tag{3.22}$$

is the value of the function $R(kd)$ at $k = k_c$ and $1 - |\Gamma(k)|^2 = \mathcal{O}(k^4)$ as $k \to 0$. In order to validate this model, the mismatch is compared between the model using

appropraite values k_c and Q values and full-wave simulation results using FEKO. In FEKO, a dipole of length $l = 0.2$m over an infinite conducting ground plane is simulated. The dipole is fed at the center as shown in Figure 3.6.

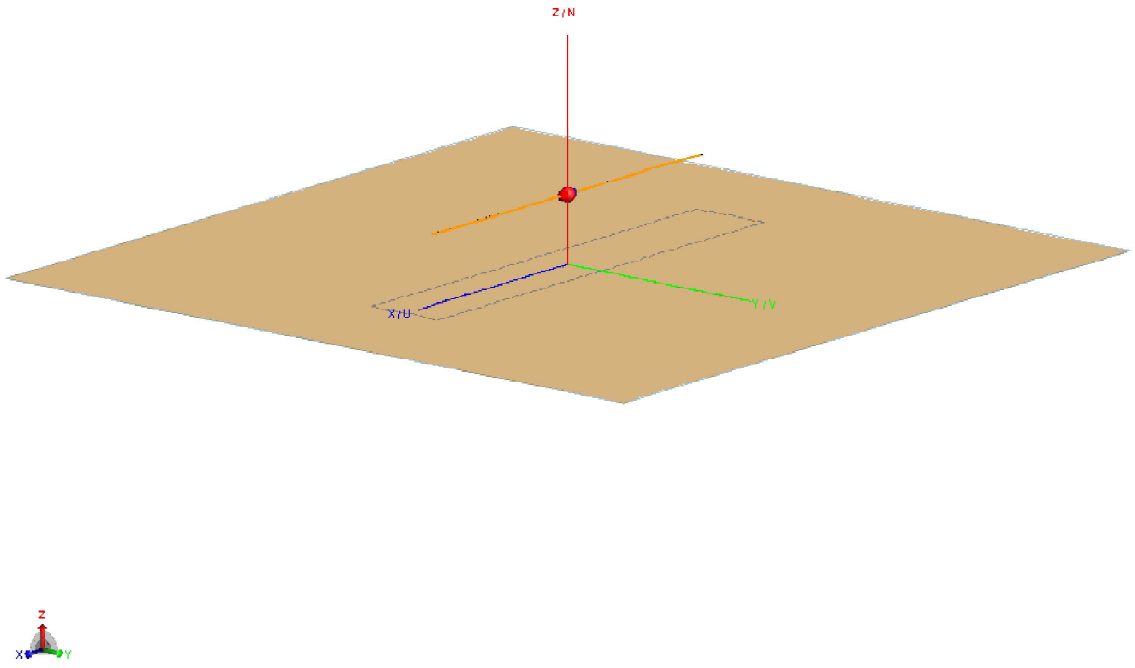

Figure 3.6. A thin wire dipole above PEC in FEKO.

The simulated input impedance was post processed to find the mismatch factor. This process is repeated for different ground separation d. Figure 3.7 shows a comparison of the model and the simulated impedance mismatch factors for three different values of d. A reasonable agreement was obtained in all test cases, validating the accuracy of (3.21).

Now that this model (3.21) has been validated, (3.17) and (3.21) were entered into the integral identity in (3.16). The resulting expression is

$$\int_0^\infty \frac{dk}{k^2(1+(\frac{Q}{2})^2(\frac{k}{k_c}-\frac{k_c}{k})^2)} \approx \frac{R(k_c d)k_c^2\eta_{abs}}{2}(\bar{e_t}^*.\gamma_{be}.\hat{e}^i). \tag{3.23}$$

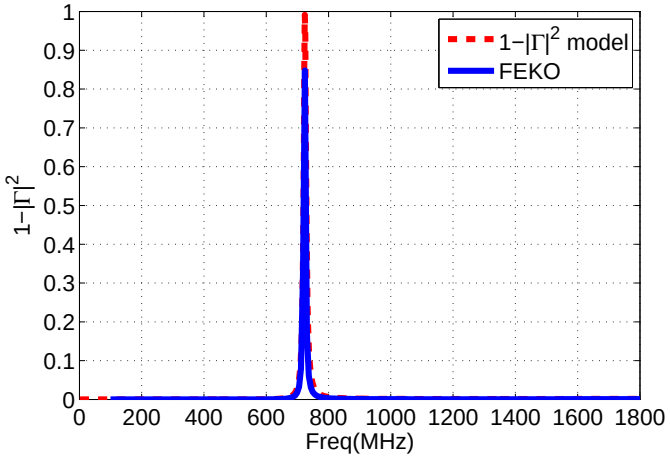

(a)

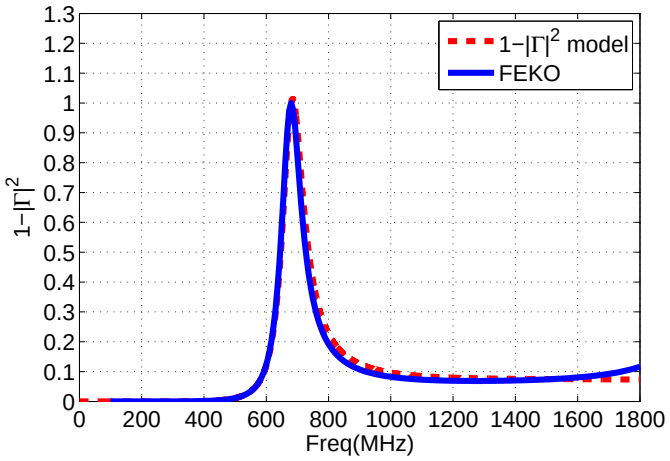

(b)

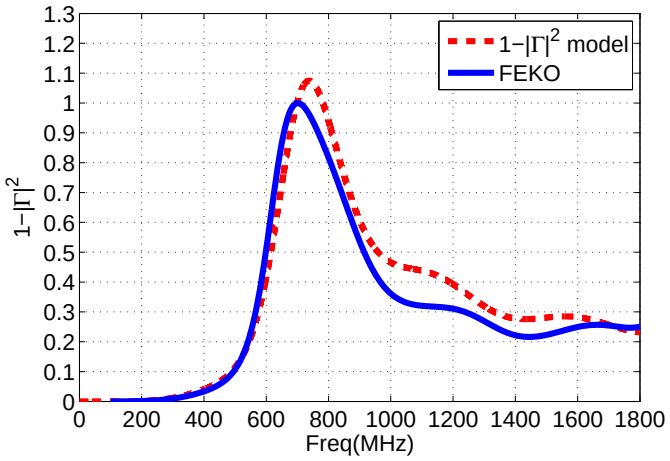

(c)

Figure 3.7. Comparison of $1 - |\Gamma(k)|^2$ at different distance d (a) $d = 0.025$ m. (b) $d = 0.125$ m. (c) $d = 0.875$ m.

This is an indefinite integral for deriving a lower bound on Q. The integral can be evaluated in a closed form, resulting in an expression showing the lower bound of Q

$$Q \approx \frac{\lambda_c^3}{R(k_c d) 4\pi^2 \eta_{abs} (\bar{e_t}^* . \gamma_{be} . \hat{e}^i)}. \tag{3.24}$$

Proof of the integral evaluation can be found in appendix A. As stated earlier, η_{abs} =0.5 can be used, while $R(k_c d)$ and λ_c are the respective values at the resonant design frequency. The polarizability($\boldsymbol{\gamma}_{be}$) represents physical(geometrical and material) properties of the antenna, which can be evaluated numerically for an antenna of interest.

3.3 Numerical Result

The derived resonance Q lower bound in (3.24) is tested for a thin-wire dipole antenna using simulations. Using the closed form expression of the Q lower bound, numerical results were generated for a physcial antenna at a different distance d above the PEC ground plane. We considered dipole of length l = 0.2m, and wire radius a = 1.0mm.

In order to evaluate the theoretical Q lower bound(3.24), the polarizability must be obtained for the values of d considered. At each d, the polarizability was obtained using COMSOL Multiphysics 4.3, which is a numerical analysis package based on the finite element method. In COMSOL, the two-antenna configuration in Figure 3.2 was analyzed to find the electrostatic polarizability, which requires evaluation of a surface integral over antenna surface. Only the electrostatic polarizability of the antenna needs to be obtained; the magenetostatic polarizability of the thin-wire geometry under consideration is equal to zero. Figure 3.8 shows the electric polarizability as a

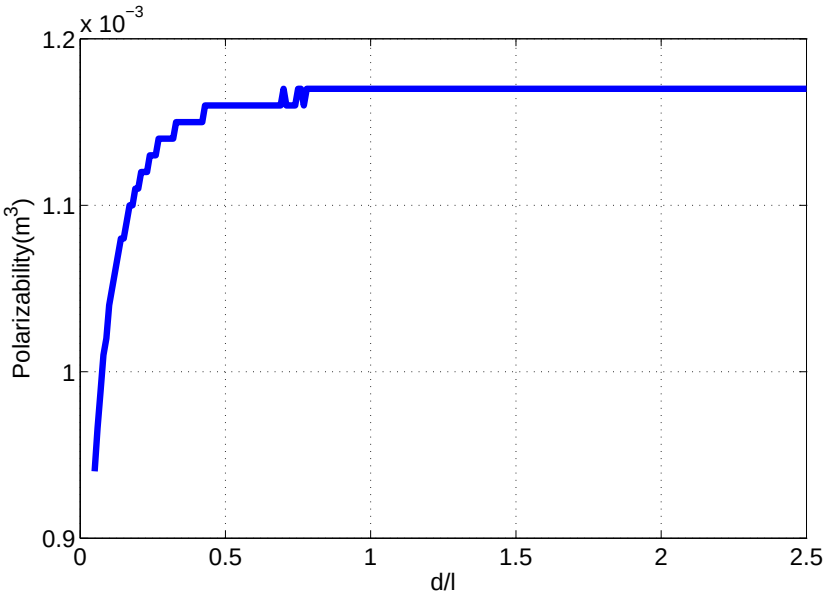

Figure 3.8. The electric polarizability of the dipole above PEC at different ground separation d.

function of the ground separation d. As d is increased, the polarizability converges to a constant value of 1.17 m^3. This makes sense because at larger ground separations from the ground plane, both the image and the real dipole antennas are far apart from each other, so that their interaction is negligible. At smaller d, the polarizability decreases with decreasing d because two antenna with a close separation behaves like a single antenna with a cross section that is twice as large as the individual antenna. After obtaining the polarizability values for different distance d, the Q lower bound can be evaluated for a wide range of electrical separation from the ground plane, characterized by $k_c d$ and the electrical length of the dipole quantified by $k_c l$. A surface color plot of Q is obtained as function of the dipole electrical length and the electrical ground separation as shown in Figure 3.9.

In order to validate the predicted Q lower bound, a half-wave dipole antenna is simulated and its resonance Q is evaluated from the input reflection coefficient. An half-wave dipole corresponds to $k_c l = \pi$, and the predicted lower bound can be read from Figure 3.9 along the corresponding horizontal line. The predicted Q bound are

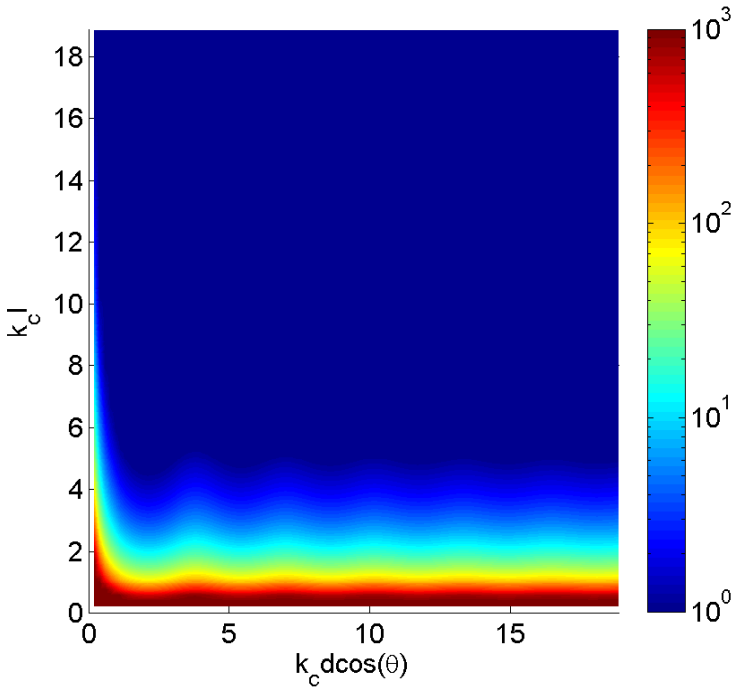

Figure 3.9. Surface plot of $k_c l$, $k_c d$ and Q for a dipole above a PEC ground plane.

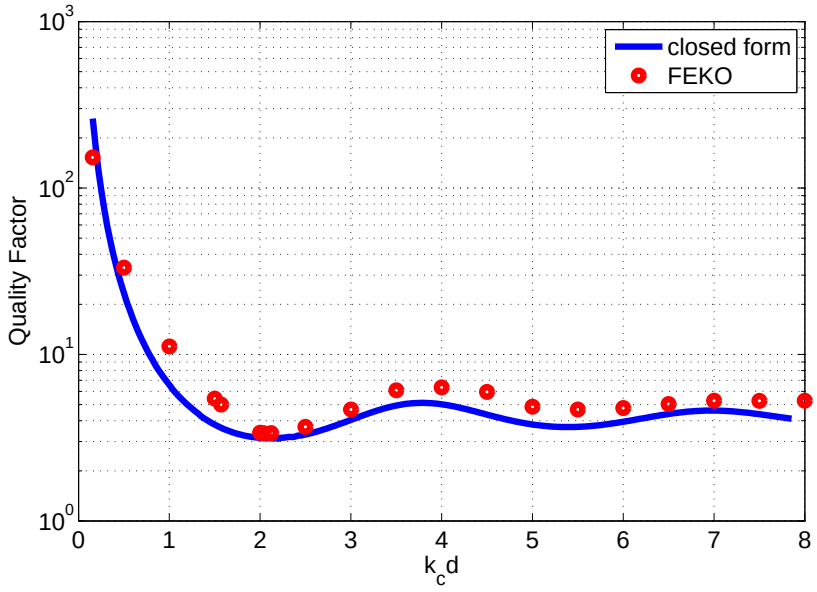

Figure 3.10. Comparison of Q from FEKO simulation and closed form at $k_c l = \pi$.

compared with the simulation results obtained from FEKO in the Figure 3.10. The predicted and simulated Q values are close to each other, validating the derived Q lower bounds.

It is interesting to note that the lowest Q corresponding to the broadest bandwidth for this dipole antenna over a PEC ground is predicted around a ground separation $k_c d = 2$. This corresponds to a distance of 0.3λ from the conducting ground plane for a simulated dipole. This is an interesting result because a conductor-backed dipole is typically designed with a quarter-wave ground separation. It means that the typical quarter-wave separation is not optimal from the bandwidth point of view.

Table 3.2. Q of a dipole above a PEC ground for different distance(d) evaluated at -3dB.

Distant(d)	f_1(MHz)	f_2(MHz)	f_c(MHz)	$1/Q$	Q
0.1	590	877.6	719.57	0.200	5
0.11	584.1	950.8	745.23	0.246	4.065
0.12	579.1	1013	765.92	0.284	3.521
0.13	575.4	1034	771.3	0.298	3.356
0.135	574.5	1032	769.99	0.297	3.367
0.14	573.6	1027	767.5	0.296	3.378
0.15	572.6	1005	758.59	0.285	3.509
0.16	574.3	980.7	750.48	0.271	3.690
0.17	577	953.8	741.85	0.254	3.937

To make a quantitative comparison, the Q values evaluated from the reflection coefficient Γ from FEKO simulations at different ground separations around $d = \lambda/4$ are compared. Table 3.2 confirms the lowest Q occurs at $d = 0.13$m. Hence, from both predicted and simulated Q values we conclude that the broadest bandwidth is achieved at a ground separation of $d \approx \lambda/3$. The fractional bandwidth is improved from 40.0% of the quater-wave separation case to 60%.

3.3.1 *Q* Comparison for a Small Antenna

In order to evaluate the effect of ground plane for electrically small antennas, the Q values for a small antenna ($k_c l = 1$) in free space is compared with the Q when backed by a conducting ground plane. The Q expression for an antenna of arbitrary material composition in free space is found from [11]

$$\frac{D}{Q} \leq \frac{\eta(-\hat{k}, \hat{e}) k_c^3}{2\pi} \left(\hat{e} \cdot \gamma_\infty \cdot \hat{e} + \left(\hat{k} \times \hat{e} \right) \cdot \gamma_\infty \cdot \left(\hat{k} \times \hat{e} \right) \right), \tag{3.25}$$

where the high-contrast polarizability dyadics γ_∞ is obtained using PEC for the antenna material. From (3.25) $D = 1.5$ can be used for electrically small dipoles to find the Q bound for free space antennas.

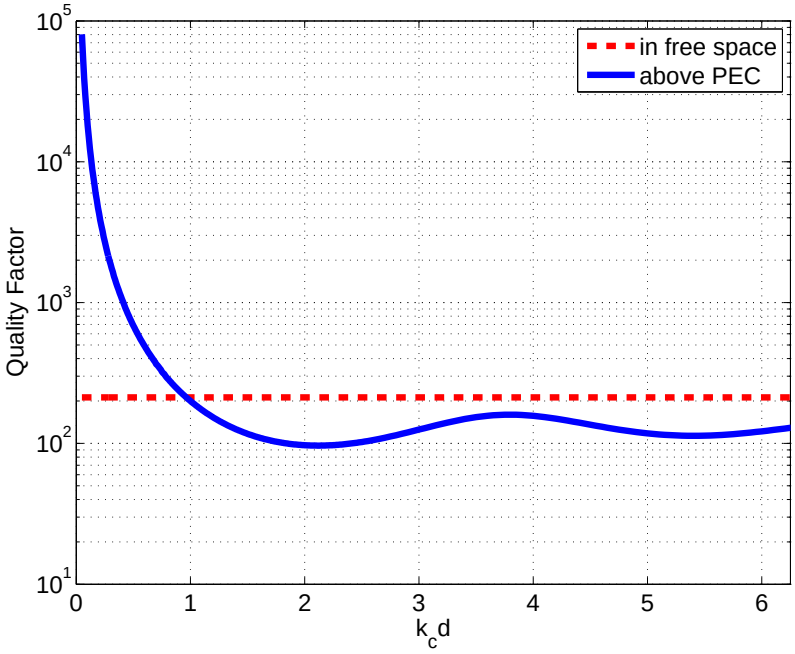

Figure 3.11. Comparison of resonance Q values for the dipole in free space and the same antenna over a ground plane of $k_c l = 1$.

The free space Q has been evaluated, and it is compared with that of the same antenna over a ground plane in Figure 3.11 with respect to ground plane. It is noted that, at lower $k_c d$, the Q of a conductor backed dipole is higher than that of the

same antenna in free space. As $k_c d$ is increased the Q reduces below the free space counterpart.

CHAPTER 4

DIPOLE ABOVE A DIELECTRIC HALF SPACE

4.1 Approximate Integral Identity for a Dipole above Dielectric Half Space

Now let's consider a horizontal dipole placed above a dielectric half space as shown in Figure 4.1.

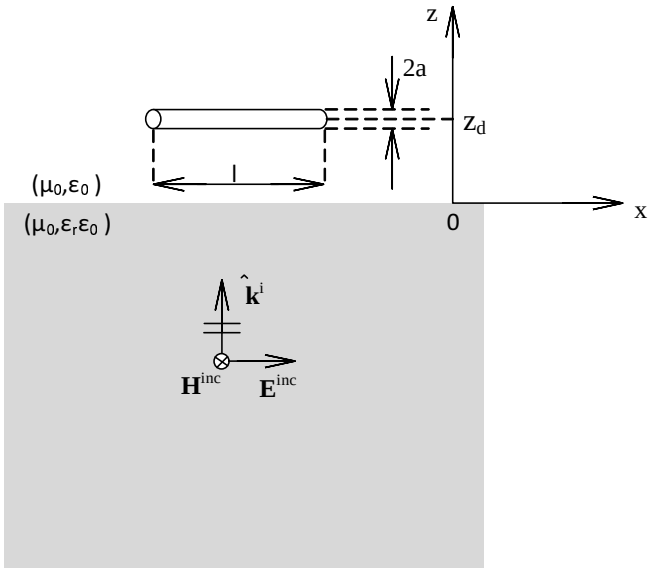

Figure 4.1. A thin wire dipole above a dielectric half space.

An approximate integral equation for the extinction cross section for this dipole is derived, which will be used to derive a lower bound expression for quality factor Q. In a case where two different media are present in addition to the antenna, the incident field onto the antenna is defined as the total field generated by the original source field in the absence of the antenna, but in the presence of the different media. The

scattered field is the difference between the total field(with both the media and the antenna present) and the incident field. Consider a linearly-polarized plane wave normally incident on the free space dielectric interface from the dielectric side having a perfect polarization match with a dipole. We define the original source fields as

$$\mathbf{E}^{inc} = \hat{x}E_0 e^{-jkz}, \text{ and } \mathbf{H}^{inc} = \hat{y}H_0 e^{-jkz}, \tag{4.1}$$

where E_0 is a complex amplitude and $H_0 = E_0/\eta$. In addition k and η are the wavenumber and the intrinsic impedance of the incident(dielectric) medium respectively. The source-field nature is indicated by the superscript 'inc.' Now the incident fields on the antenna are those of the transmitted plane wave, given by

$$\mathbf{E}^{i} = \hat{x}E_0 T e^{-jk_0 z}, \text{ and } \mathbf{H}^{i} = \hat{y}H_0(2-T) e^{-jk_0 z}, \tag{4.2}$$

where $T = 2\eta_0/(\eta+\eta_0)$ is the transmission coefficient, k_0 is the free space wavenumber, and η_0 is the free space intrinsic impedance. There will be a reflected plane wave inside the dielectric propagating in the $-z$ direction, but it is not of concern from the antenna's viewpoint. With this definition of the incident fields, the extinction cross section of the antenna will account for the antenna's property in the presence of a medium interface.

The total electric and magnetic fields $(\mathbf{E}, \mathbf{H})$ can be decomposed into the incident $(\mathbf{E}^i, \mathbf{H}^i)$ fields and the scattered fields $(\mathbf{E}^s, \mathbf{H}^s)$. The extinction cross section is the sum of the absorption cross section and the scattering cross section given by

$$\sigma_{ext}(k_0) = \sigma_a(k_0) + \sigma_s(k_0). \tag{4.3}$$

Both the absorption and scattering cross sections can be written in terms of the power delivered to the load P_L and the power scattered by the antenna P_S respectively as

$$\sigma_a(k_0) = \frac{2\eta}{|E_0|^2} P_L, \text{ and } \sigma_s(k_0) = \frac{2\eta}{|E_0|^2} P_S. \tag{4.4}$$

Note that the powers need to be normalized by the power density of the original source field. The powers P_L and P_S can be expressed as the powers leaving a closed surface bounding the antenna using the total fields and using the scattered fields, respectively, as

$$P_L = -\frac{1}{2} \oint_S \text{Re}\{\mathbf{E} \times \mathbf{H}^*\} \cdot \hat{n} ds', \text{ and } P_S = \frac{1}{2} \oint_S \text{Re}\{\mathbf{E}^s \times \mathbf{H}^{s*}\} \cdot \hat{n} ds', \tag{4.5}$$

where S denotes a close surface that encloses the antenna. Using (4.5), the extinction cross section is expressed as

$$\sigma_{ext}(k_0) = -\frac{\eta}{|E_0|^2} \text{Re}\left\{ \oint_S (\mathbf{E}^i \times \mathbf{H}^* + \mathbf{E} \times \mathbf{H}^{i*}) \cdot \hat{n} ds' \right\}. \tag{4.6}$$

Equation (4.2)can be substituted into (4.6) to give

$$\sigma_{ext}(k_0) = \frac{\eta}{|E_0|^2} \text{Re}\left\{ \hat{x} E_0^* T^* \cdot \hat{z} \times \oint_S \left[(\hat{n} \times \mathbf{H}) \times \hat{z} + \frac{1}{\eta_0} (\hat{n} \times \mathbf{E}) \right] e^{jk_0 z'} ds' \right\}. \tag{4.7}$$

The expression in the bracket in (4.7) can be expanded, and the extinction cross section becomes

$$\begin{aligned} \sigma_{ext}(k_0) = \frac{\eta}{|E_0|^2} \text{Re}\Bigg\{ & \hat{x} \frac{\eta}{\eta_0} E_0^* T^* \cdot jk_0 \hat{z} \times \\ & \oint_S \left[\hat{z} \times \mathbf{r}'(\hat{z} \cdot \hat{n} \times \eta_0 \mathbf{H} - \hat{n} \cdot \mathbf{E}) - \mathbf{r}'(\hat{z} \cdot \hat{n} \times \mathbf{E} + \hat{n} \cdot \eta_0 \mathbf{H}) \right] e^{jk_0 z'} ds' \Bigg\}. \end{aligned} \tag{4.8}$$

Now, we expand the total fields as a power series with respect to k_0, and keep the terms of the lowest-order to find the low-frequency asymptotic expression. The fields

approach their static quantities, allowing them to be expressed in terms of static potential as

$$\mathbf{E} = \mathbf{E}_0 = -\nabla\Phi_0, \text{ and } \mathbf{H} = \mathbf{H}_0 = -\nabla\Psi_0, \tag{4.9}$$

where Φ_0 and Ψ_0 are the electrostatic and magnetostatic potentials respectively. The low frequency asymptotic expression for σ_{ext} can be written as

$$\begin{aligned}\sigma_{ext}(k_0) &= -\frac{1}{|E_0|^2}\mathrm{Re}\left\{\hat{x}\frac{\eta}{\eta_0}E_0^* T^* \cdot jk_0\left(\hat{z}\times\hat{z}\times\frac{\mathbf{p}}{\epsilon_0} + \hat{z}\times\eta_0\mathbf{m}\right) + \mathcal{O}(k^2)\right\} \\ &= \frac{1}{|E_0|^2}\mathrm{Re}\left\{jk_0\frac{\eta}{\eta_0}T^* E_0^*\left(\hat{x}\cdot\frac{\mathbf{p}}{\epsilon_0} + \hat{y}\cdot\eta_0\mathbf{m}\right) + \mathcal{O}(k^2)\right\}, \quad k_0 \to 0,\end{aligned} \tag{4.10}$$

where $\mathbf{p}$ and $\mathbf{m}$ are the electrostatic and magnetostatic dipole moments, respectively. They are defined by

$$\mathbf{p} = \epsilon_0 \oint_S \left(\hat{n}\Phi_0 - \mathbf{r}'\frac{\partial\Phi_0}{\partial n}\right) ds', \text{ and } \mathbf{m} = \frac{1}{\eta_0}\oint_S \left(\hat{n}\Psi_0 - \mathbf{r}'\frac{\partial\Psi_0}{\partial n}\right) ds'. \tag{4.11}$$

Using the relative permittivity ϵ_r of the medium (4.10) can be rewritten as

$$\sigma_{ext}(k_0) = \mathrm{Re}\left\{jk_0\frac{1}{\sqrt{\epsilon_r}}T^*\left(\hat{x}\cdot\frac{\mathbf{p}/\epsilon_0}{|E_0|} + \hat{y}\cdot\frac{\eta_0\mathbf{m}}{\eta|H_0|}\right) + \mathcal{O}(k^2)\right\}, \quad k_0 \to 0, \tag{4.12}$$

where $E_0 = \eta H_0$ has been used. A closed contour integral of $\sigma_{ext}(k_0)/k_0^2$ over a contour in the lower half plane of the complex-k plane of Figure 2.3 can be performed using the Cauchy integral theorem, resulting in an integral identity

$$\int_0^\infty \frac{\sigma_{ext}(k_0)}{k_0^2}dk_0 = \frac{\pi}{2\sqrt{\epsilon_r}}T\left(\hat{x}\cdot\frac{\mathbf{p}/\epsilon_0}{|E_0|} + \hat{y}\cdot\frac{\eta_0\mathbf{m}}{\eta|H_0|}\right). \tag{4.13}$$

The fact that the transmission coefficient T at the dielectric-free space interface is a real-valued constant for lossless dielectric has been used. Since $\sigma_{ext}(k_0)$ is not related to the forward scattering coefficient due to the presence of the dielectric half space,

(4.13) is not expected to hold exactly. The approximate nature of (4.13) can be understood by considering a related problem that has an exact integral identity for the extinction cross section. For this purpose, consider the same antenna in free space without the dielectric half space, subject to an x-directed incident field of electric field amplitude $(1+\Gamma)E_0$. The associated extinction cross section $\sigma_{ext}(k_0)$ satisfies the integral sum rule

$$\int_0^\infty \frac{\sigma_{fs,ext}(k_0)}{k_0^2} dk_0 = \frac{\pi}{2\sqrt{\epsilon_r}} T \left(\hat{x} \cdot \frac{\mathbf{p}_{fs}/\epsilon_0}{T|E_0|} + \hat{y} \cdot \frac{\mathbf{m}_{fs}}{T|H_0|} \right), \tag{4.14}$$

where $\mathbf{p}_{fs}$ and $\mathbf{m}_{fs}$ are the induces dipole moments. Re-scaling $\sigma_{fs,ext}$ with the incident power density from the dielectric medium in Figure 4.1, (4.14) becomes

$$\begin{aligned} \int_0^\infty \frac{1}{k_0^2} \left[\sigma_{fs,ext}(k_0) \frac{|T|^2}{\eta_0/\eta} \right] dk_0 &= \frac{\pi}{2} \frac{|T|^2}{\eta_0/\eta} \left(\hat{x} \cdot \frac{\mathbf{p}_{fs}/\epsilon_0}{T|E_0|} + \hat{y} \cdot \frac{\mathbf{m}_{fs}}{T|H_0|} \right) \\ &= \frac{\pi}{2\sqrt{\epsilon_r}} T \left(\hat{x} \cdot \frac{\mathbf{p}/\epsilon_0}{|E_0|} + \hat{y} \cdot \frac{\eta_0 \mathbf{m}}{\eta |H_0|} \right). \end{aligned} \tag{4.15}$$

Comparing (4.13) and (4.15), it can be concluded that (4.13) is expected to be accurate when $\mathbf{p}$ and $\mathbf{m}$ approach $\mathbf{p}_{fs}$ and $\mathbf{m}_{fs}$, respectively, i.e., when the induced static dipoles in the presence of a dielectric half space are similar to those in the materials absence. Hence we expect the agreement of both sides of (4.13) will improve as the dipole is positioned away from the interface and deteriorate as the dipole is moved closer to the interface. The validity of the identity can be numerically tested. It is tested for a dielectric material of $\epsilon_r = 40$, which was chosen to represent the permittivity of muscle [16]. The geometry of the thin-wire PEC antenna is given by $l = 0.5$ m and $a = 2.5$ mm. The z-coordinate of the dipole axis is z_d. The magnetic dipole moment on the right hand side of identity is negligible and thus it can be dropped because the antenna is thin and perfectly conducting. The lhs of (4.13) is obtained from frequency-swept simulation using FEKO, and the rhs of (4.13) is

obtained from COMSOL. Figure 4.2 illustrates the simulation setup in FEKO and COMSOL. In FEKO, $\sigma_{ext}(k_0)$ was obtained from the scattered power as a function of frequency, and then (4.4) was used. After getting $\sigma_{ext}(k_0)$, numerical integration was performed. In COMSOL, a static background electric field is applied to a sufficiently large cuboidal simulation volume to imitate an unbounded space and the strength of the induced dipole moment was obtained using (B.1). The Table4.1 lists the agreement between the lhs and rhs of the identity. The agreement slightly deteriorates as the z_d is lowered toward zero, but we obtain an overall reasonable agreement over the range of z_d considered. As in the case of a wire dipole backed by a PEC ground, the

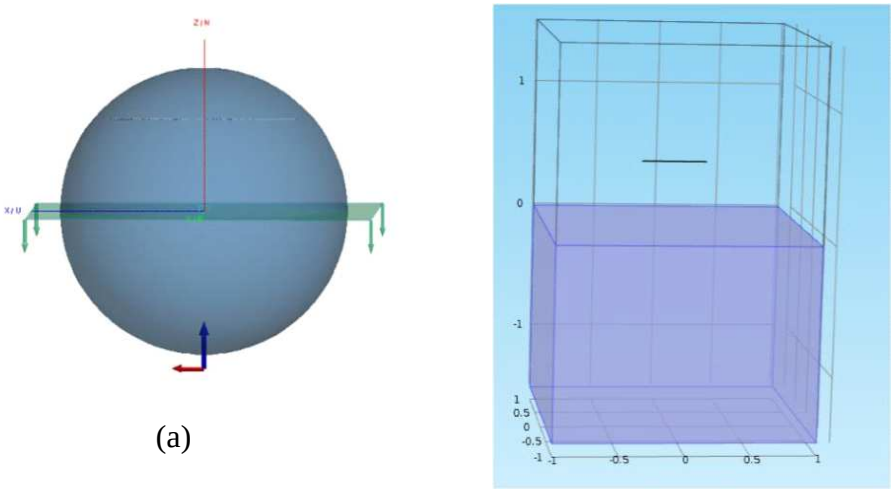

Figure 4.2. A thin wire dipole above a dielectric half space in (a) FEKO (b) COMSOL.

$\sigma_{ext}(k_0)$ in the integral can be replaced with equality

$$\sigma_{ext}(k_0) \approx \frac{\sigma_a(k_0)}{\eta_{abs}}. \tag{4.16}$$

The absorption cross section, $\sigma_a(k_0)$, can be replaced with

$$\sigma_a(k_0) = A_e(k_0) = \frac{\lambda^2}{4\pi} D(k_0)(1 - |\Gamma(k_0)|^2) = \frac{\pi}{\epsilon_r k_0^2} D(k_0)(1 - |\Gamma(k_0)|^2), \tag{4.17}$$

Table 4.1. Validation of the integral identity for a wire dipole above a dielectric half space for $\epsilon_r = 40$.

Separation(z_d)	LHS	COMSOL($\frac{\mathbf{p}}{\epsilon_0}$)	RHS	Percent diff.
1	0.0131	0.0183	0.0136	3.7
0.55	0.0131	0.0184	0.0136	3.7
0.5	0.0131	0.0184	0.0136	3.7
0.45	0.0131	0.0184	0.0136	3.7
0.35	0.0131	0.0184	0.0136	3.7
0.30	0.0131	0.0184	0.0137	4.4
0.25	0.0131	0.0185	0.0137	4.4
0.20	0.0131	0.0186	0.0138	5.1
0.15	0.0133	0.0188	0.0139	4.3
0.10	0.0136	0.0193	0.0143	5.0
0.05	0.0146	0.0209	0.0155	5.8
0.04	0.0152	0.0217	0.0161	5.6
0.03	0.0160	0.0228	0.0169	5.3
0.02	0.0176	0.0323	0.0187	5.9
0.01	0.0219	0.0323	0.0239	8.4

where $1 - |\Gamma(k_0)|^2$ is the impedance mismatch factor, D is the directivity, λ is the wavelength, ϵ_r is the relative permittivity of the dielectric, and k_0 is the free space wavenumber. Here, it should be remembered that the wavelength is the one in medium where the directivity is evaluated which is the wavelength inside the dielectric. When all the substitutions are made, the integral identity in (4.13) becomes

$$\frac{\pi}{\eta_{abs}} \int_0^\infty \frac{D(k_0)(1 - |\Gamma(k_0)|^2)}{k_0^4} dk_0 \approx \frac{\pi\sqrt{\epsilon_r}}{2} T \left(\hat{x} \cdot \frac{\mathbf{p}/\epsilon_0}{|E_0|} + \hat{y} \cdot \frac{\eta_0 \mathbf{m}}{\eta |H_0|} \right). \tag{4.18}$$

Now, the next step is obtaining a model for the mismatch $1 - |\Gamma|^2$ and the directivity D. This is the focus of the following sections.

4.2 Model for $1 - |\Gamma(k_0)|^2$

In order to derive a model for this problem, we start from the model of $1 - |\Gamma|^2$ for a resonant antenna in free space around the resonance frequency and modify it to fit

the behavior of the mismatch with respect to frequency. Within the frequency band of resonance, the mismatch factor can be accurately modeled using (3.19) in terms of the center wavelength k_{0c} and the resonance quality factor Q. In the integral on the lhs of (4.18), we find that the contribution to the integral is not dominated by the resonance frequency band and the contribution from the low frequency range is non-negligible. An approximate low-frequency behavior of $1-|\Gamma|^2$ can be accounted for by matching the order of frequency dependence as $k_0 \to 0$. Therefore, by introducing a factor $(\frac{k_0}{k_{0c}})^2$ to the standard narrowband response (3.19), the resonant behavior of the mismatch factor around the resonance frequency is preserved while a correct low frequency dependence is accounted for. Hence, the model for the mismatch is set to

$$1-|\Gamma(k_0)|^2 = \left(\frac{k_0}{k_{0c}}\right)^2 \frac{1}{1+(\frac{Q}{2})^2(\frac{k_0}{k_{0c}}-\frac{k_{0c}}{k_0})^2}. \tag{4.19}$$

This model has the correct order of $\mathcal{O}\left(k_0^4\right)$ at low frequency. This model is compared with the mismatch from FEKO simulation for different dipole position z_d in Figure 4.3. The model matches the impedance mismatch factor from simulation around resonance as well as in the low frequency limit. The model also closely follows the simulated mismatch as the frequency is increased from zero to the resonance frequency. Therefore, it is a good mathematical model that can be used for $1-|\Gamma|^2$ in (4.13).

4.3 Model for $D(k_0)$

The directivity D in the integrand of (4.18) is a function of frequency. Here, it is important to remember that this directivity is in a fixed direction rather than the maximum directivity. This fixed direction is the direction of the incoming wave, which is the z axis direction ($\theta = \pi$) for this dipole in free space.

In the study of directive properties of antennas for transmission into material half space, Smith considered the case where a Hertzian dipole radiates into a half space

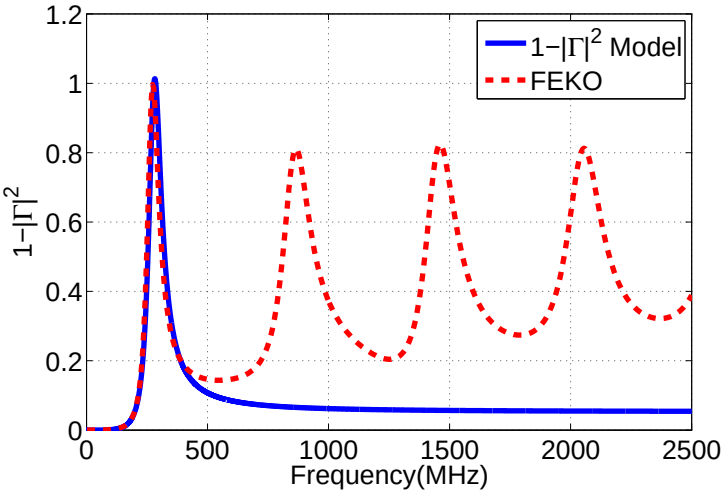

(a)

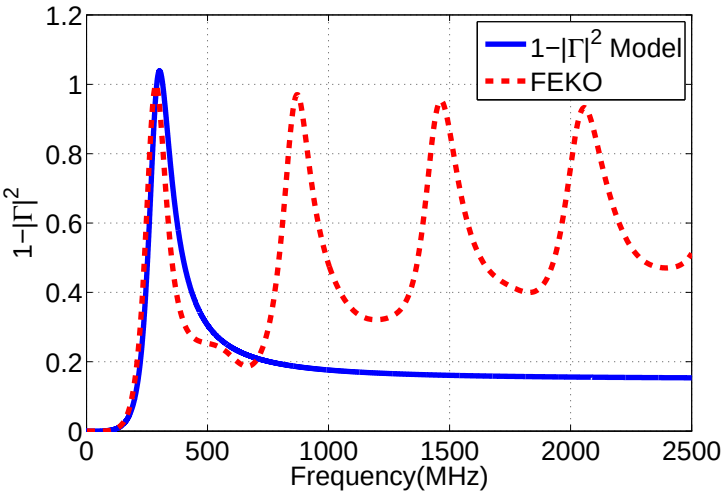

(b)

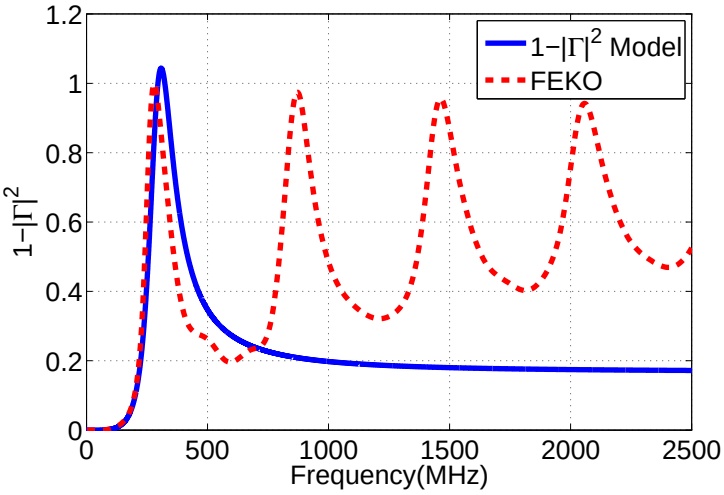

(c)

Figure 4.3. Comparison of $1 - |\Gamma(k_0)|^2$ at different distance z_d. (a) $z_d = 0.15$ m. (b) $z_d = 0.5$ m. (c) $z_d = 0.85$ m.

as illustrated in Figure 4.4 [17]. We can evaluate the directivity looking normally into the dielectric half space for D to use in (4.18). Smith focused on the space

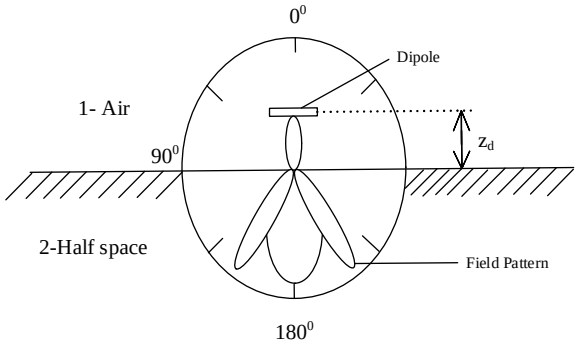

Figure 4.4. Smith's directive properties of antennas transmitting into half space.

wave characteristics rather than surface waves that flows along the interface between the half space and the adjacent medium. Fields of an antenna over a half space are expressed as an integral over 2-D spectra of propagating and evanescent plane waves. The directivity of a Hertzian electrica dipole antenna over a half space is expressed as [17]

$$D(\theta) = \frac{4\pi\hat{r} \cdot \mathrm{Re}[\vec{S}_c^r(r,\theta)]}{\iint \hat{r} \cdot \mathrm{Re}[\vec{S}_c^r(r,\theta,\phi)d\Omega} = \frac{2k_1^2|\vec{A}^+(\vec{K}=0)|^2}{\pi\zeta_2(1+k_{12})^2 P_{in}}. \tag{4.20}$$

The second expression in (4.20) is given in terms of the spectral density $\vec{A}^+$. In (4.20), $\hat{r}$ is the unit vector in the direction from the antenna to a far-field position in the dielectric medium, $\vec{S}_c^r(r,\theta)$ is the complex far-zone Poynting vector, $\vec{A}^+$ is the spectral density that has both parallel and normal component, $k_{12} = \frac{k_1}{k_2}$ is the ratio of the wavenumbers in the two media (k_1 is the same as k_0 in this work), ζ_2 is the impedance of the half space, and P_{in} is the input power. The directivity for horizontal electric dipole above a dielectric half space is written as [17]

$$D_e = \frac{8k_{21}}{(1+k_{12})^2}\left\{\frac{4}{3} - \int_0^1 \left[R_\parallel - \left(\frac{k_1}{\gamma_1}\right)^2 R_\perp\right]\cdot\cos(2\gamma_1 h)\rho d\rho \right. \\ \left. -\frac{1}{k_1}\int_1^{k_{21}} |\gamma_1| e^{-2|\gamma_1|h}\cdot\left[\mathrm{Im}(R_\parallel) + \left|\frac{k_1}{\gamma_1}\right|^2 \mathrm{Im}(R_\perp)\right]\rho d\rho\right\}^{-1}. \tag{4.21}$$

In (4.21), $k_{12} = k_1/k_2$, $k_{21} = k_2/k_1$, the parallel reflection coefficient $R_\parallel(K) = (k_2^2\gamma_1 - k_1^2\gamma_2)/(k_2^2\gamma_1 + k_1^2\gamma_2)$, the perpendicular reflection coefficient $R_\perp(K) = (\gamma_1 - \gamma_2)/(\gamma_1 + \gamma_2)$, the parallel transmission coefficient $T_\parallel(K) = 2k_1k_2\gamma_1/(k_2^2\gamma_1 + k_1^2\gamma_2)$, the perpendicular transmission coefficient $T_\perp(K) = 2\gamma_1(\gamma_1 + \gamma_2)$, $\gamma_1 = -\jmath\sqrt{K^2 - k_1^2}$, $\gamma_2 = -\jmath\sqrt{K^2 - k_2^2}$, $\rho = K/k_1$, and $K = \sqrt{k_x^2 + k_y^2}$. The directivity from (4.21) is compared with that from FEKO simulation for an electrically small dipole, in Figure 4.5. In FEKO simulation, a short dipole of length $l = 0.02$m is used. An excellent agreement between the theoretical and numerical results is observed at all frequencies considered. In Figure 4.5, it is noticed that directivity stays high away from the low-frequency range compared with that of the same antenna in free space, which is 1.5. This may appear counter-intuitive because of a large impedance mismatch between free space and the dielectric medium. In Figure 4.6 simulated directivity patterns from FEKO are shown for a dipole on the free space side and a dipole on the dielectric side at two frequencies. For a small dipole above the dielectric interface at $z_d = 0.5$ m, directivity patterns in the two principal planes are shown at 500 MHz and 1500 MHz in Figure 4.6 (a) and (b). Directivity is higher looking into the dielectric ($\theta = \pi$) than in the opposite direction into free space ($\theta = 0$). However, numerical results show that a larger portion of the total radiated power radiates into the free space side. Figure 4.6(c) and (d) show the directivity in the principal planes for a small dipole inside dielectric with $z_d = 0.5$ m at two frequencies. It is observed that more power is radiated into the dielectric than into free space. The same behavior occurs when a dipole antenna is placed on the interface of a lossless dielectric half space [18]. In addition, the directivity is higher into the dielectric than toward free

space. Thus, it is concluded that directivity is higher into the dielectric than into free space when the antenna is placed either on the surface of the interface, above the dielectric half space or inside the dielectric half space.

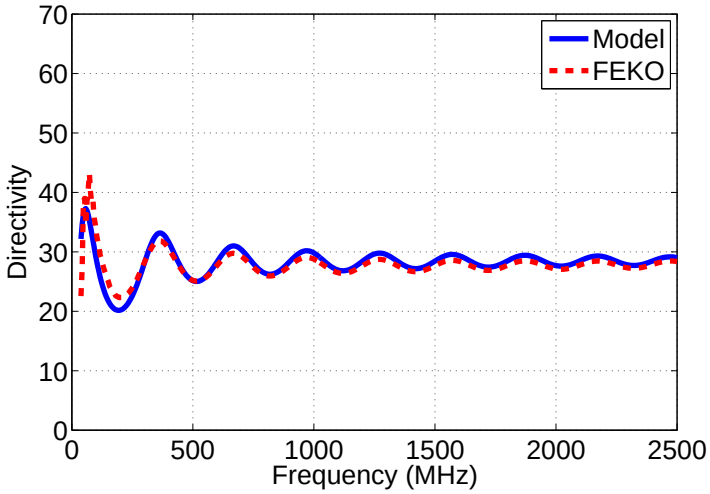

Figure 4.5. Directivity comparison between FEKO and [17] for infinitesimal dipole above half space.

Since (4.21) will be used in deriving the Q bound while practical antennas have non-negligible lengths, it is instructive to compare (4.21) with the accurate directivity of a a practical self-resonant dipole of half wavelength. This comparison is made in Figure 4.7, where a reasonable agreement is observed in the low frequency range, but not at high frequencies.

However, it should be noted that accuracy of the directivity used in developing the model in the low frequency is most important because there is a $1/k_0^4$ weight that attenuates the integrand at high frequencies in (4.18). Since the expression for D is not in a closed form, we cannot find a Q bound in a closed form by substituting the directivity expression into (4.18) as was done in the case of dipole above a PEC ground in Chapter 2. Hence the Q lower bound will be numerically generated. Numerical

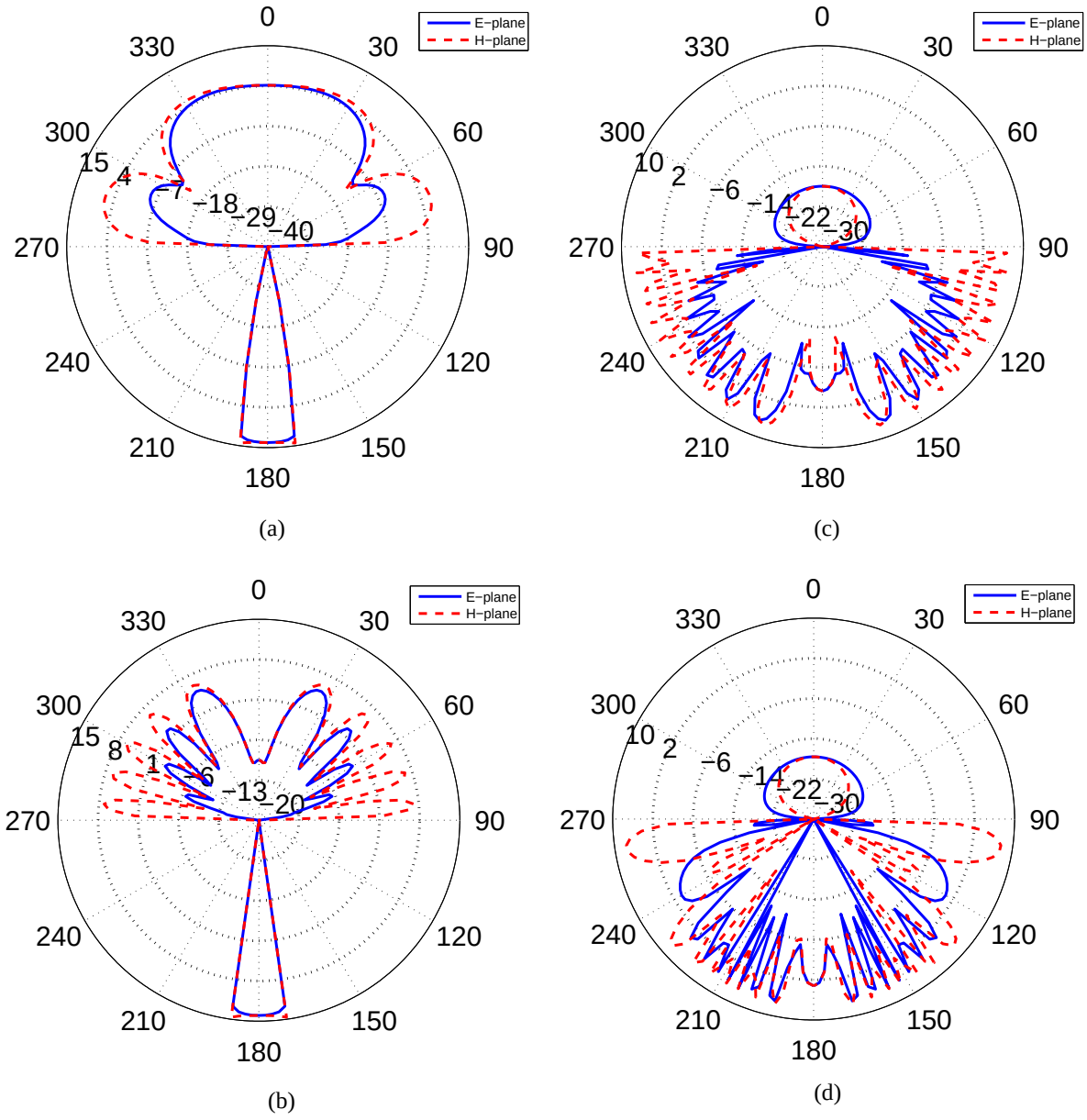

Figure 4.6. Polar plot of the directivity pattern of a dipole of length $l = 0.01\lambda$. (a) dipole above half space at 500 MHz. (b) dipole above half space at 1500 MHz. (c) dipole inside half space at 500 MHz. (d) dipole inside half space at 1500 MHz.

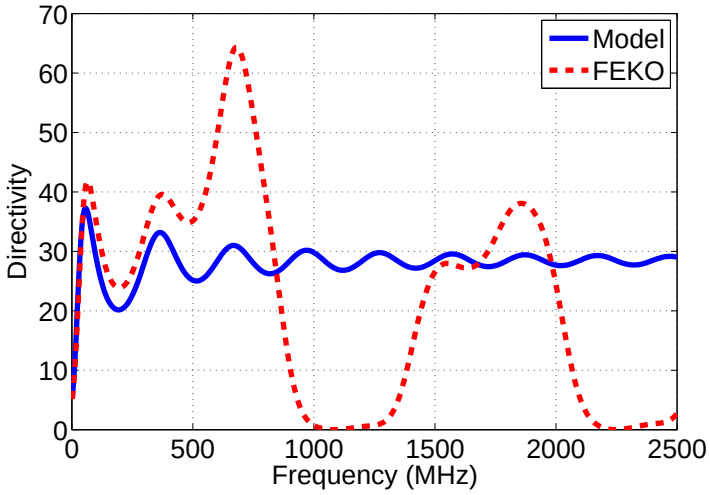

Figure 4.7. Directivity comparison between FEKO and [17] for a half-wave dipole above a dielectric half space at $z_d = 0.5$ m.

results for the resonance Q bound for a dipole antenna above a dielectric half space is considered in the next section.

4.4 Numerical Result

4.4.1 High permittivity case $\epsilon_r = 40$

In order to obtain the Q bound for this problem using (4.18), numerical integration must be performed since there is no closed form expression for the integral. Even with accurate directivity values obtained from numerical analysis, it should be checked if the model for the extinction cross section, and therefore the integrand, agrees well with full-wave simulation results of a physical antenna. For an example case of $l = 0.5$ m, $a = 2.5$ mm, $z_d = 0.5$ m, and $\epsilon_r = 40$, the extinction cross section is compared between the model and the simulation result in Figure 4.8. For the model-generated value, (4.18) with an absorption efficiency value of $\eta_{abs} = 0.5$ is used. The simulation results for σ_{ext} is generated by a receiving antenna simulation. The extinction cross section can be computed from the scattered and received power quantities from numerical analysis. In Figure 4.8, a reasonable agreement is observed. Since the model uses

the directivity of an infinitesimal dipole, the difference is attributed in part to the inaccuracy of the directivity in the model. As a check, another extinction cross section is plotted based on (4.18) and (4.17), but using the accurate directivity obtained from a transmitter simulation in FEKO. An improvement is observed for the agreement, confirming that the main source of difference is the use of (4.21) in the model of σ_{ext}. Comparison of the integrand is shown in Figure 4.9, which demonstrates a reasonable agreement between the frequency-dependent model and the accurate numerical result. For a given combination of the electrical length of the dipole, $k_{0c}l$, and the position of the dipole relative to the material interface, $k_{0c}z_d$, the value of Q can be found using (4.18). Figure 4.10 shows a color surface plot of Q with respect to $k_{0c}z_d$ and $k_{0c}l$.

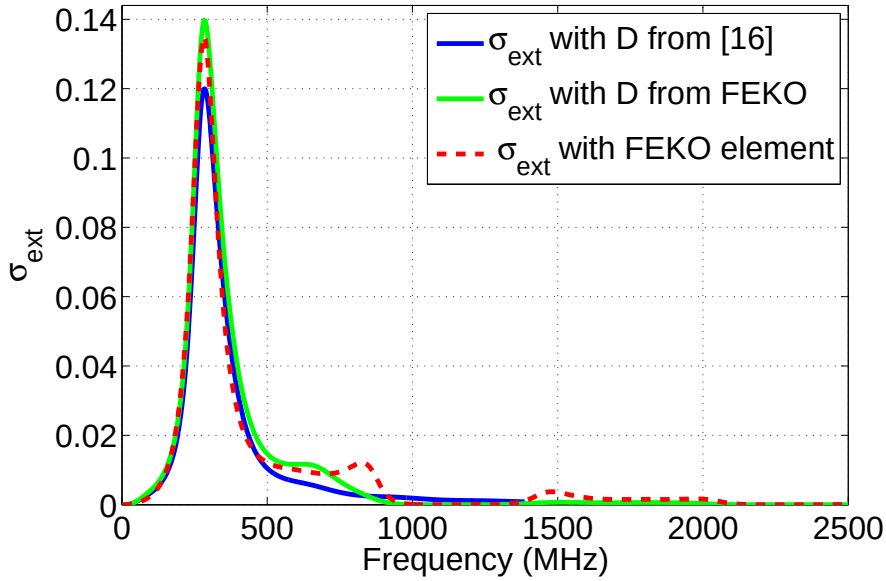

Figure 4.8. Comparison between σ_{ext} from FEKO receiving antenna, σ_{ext} using the directivity from (4.21), and σ_{ext} using the directivity from FEKO at $z_d = 0.5$ m.

To inspect the expected Q behavior for a fixed-length dipole as a function of the separation from the material interface, consider a dipole at $k_{0c}l = \pi$, which corresponds to a practical half-wave dipole. This fixed electrical length corresponds to a cut on the surface plot, and it is compared with quality factor obtained from FEKO in the Figure 4.11. It is observed that the predicted Q is close to the simulated

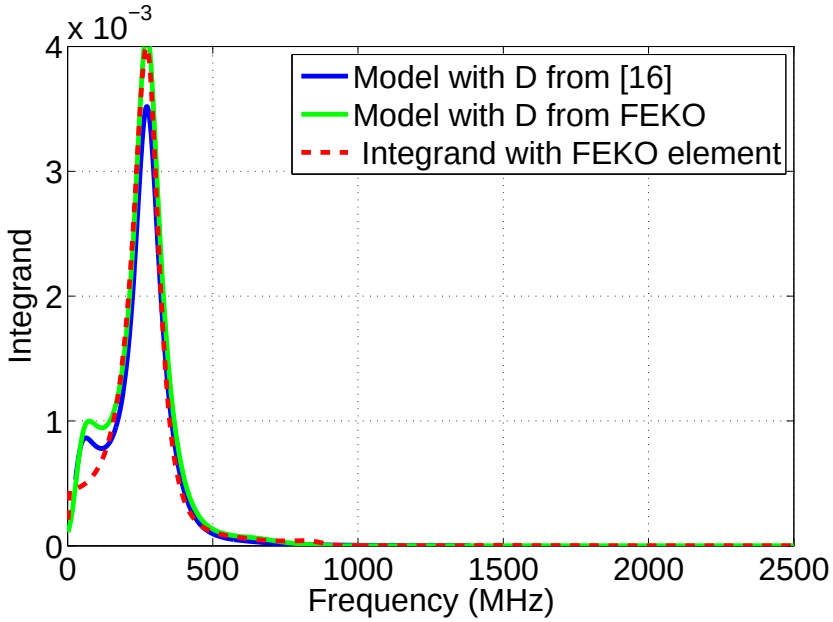

Figure 4.9. Comparison between integrand from FEKO receiving antenna, one using directivity from (4.21), and one using directivity from FEKO at $z_d = 0.5$ m.

Q and follows the same trend with respect to $k_{0c}z_d$, and also that the predicted Q is consistently lower. This is attributed to the lower value of D used in the model than that of the dipole of correct length. As a check, another Q is found numerically from (4.18) using the accurate directivity value from FEKO simulations. The associated Q values are also shown in Figure 4.11. It confirms that the slightly low directivity from (4.21) is the reason for slightly lower predicted Q values.

4.4.2 Low permittivity case $\epsilon_r = 4$

In this section, dipole Q values are predicted associated with a dielectric half space od a permittivity value in the low range. Here a value of $\epsilon_r = 4$ is chosen. First, the approximate integral identity (4.13) is tested for this permittivity value. The dipole geometry is kept at $l = 0.5$ m, $a = 2.5$ mm. Comparison of both sides of (4.13) is made in Table 4.2. Over the entire range of z_d considered, the error is 5% or less, validating the derived identity.

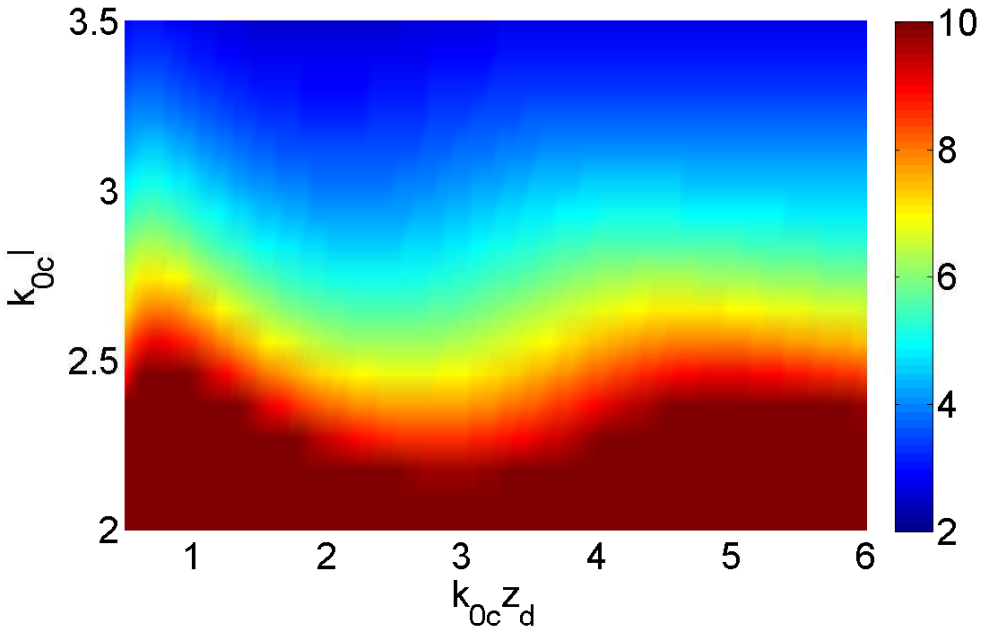

Figure 4.10. Surface plot for quality factor for dipole above a dielectric half space when $\epsilon_r = 40$.

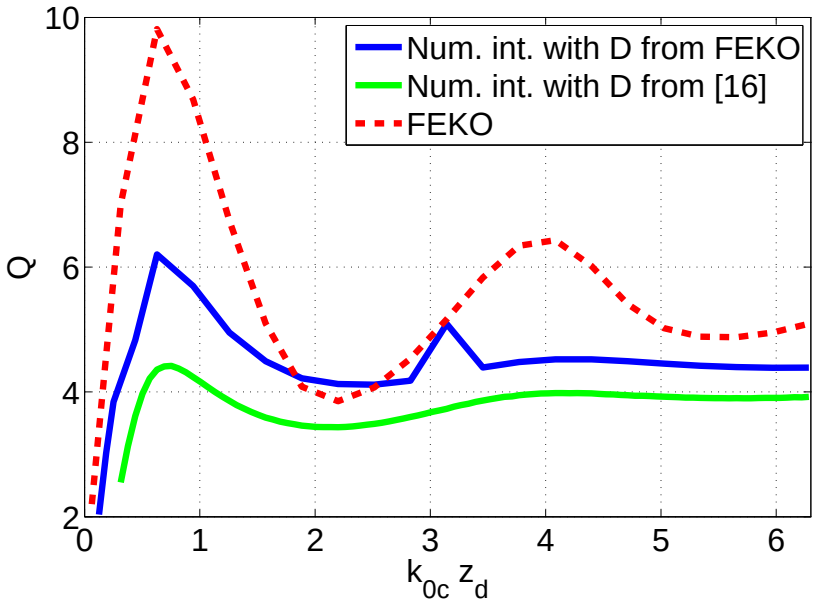

Figure 4.11. Quality factor comparison at $k_{0c}l = \pi$ when $\epsilon_r = 40$.

Using the same procedure as in the $\epsilon_r = 40$ case, a surface plot of the predicted Q

Table 4.2. Validation of integral identity for a wire dipole above a dielectric half space for $\epsilon_r = 4$.

Separation(z_d)	LHS	COMSOL($\frac{P}{\epsilon_0}$)	RHS	Percent diff.
1	0.0247	0.0183	0.0257	4.3
0.5	0.0246	0.0184	0.0257	4.3
0.45	0.0246	0.0184	0.0257	4.3
0.35	0.0246	0.0184	0.0257	4.3
0.30	0.0246	0.0184	0.0257	4.3
0.25	0.0247	0.0185	0.0258	4.3
0.20	0.0247	0.0185	0.0258	4.3
0.15	0.0249	0.0186	0.0260	1.8
0.10	0.0252	0.0189	0.0264	2.0
0.05	0.0264	0.0199	0.0278	5.0
0.04	0.0270	0.0203	0.0284	4.8
0.03	0.0279	0.0209	0.0291	4.1
0.02	0.0294	0.0221	0.0308	4.6
0.01	0.0337	0.0252	0.0352	4.3

is generated as a function of the electrical length, $k_{0c}l$, and the electrical separation to the material interface, $k_{0c}z_d$, as shown in Figure 4.12. Comparing with Figure 4.10, Q changes more slowly with respect to the separation from the material interface. The behavior of Q is inspected for a fixed length of half wavelength and the predicted Q values are compared with those obtained from full-wave FEKO simulations in Figure 4.13. The predicted Q values are close to the simulated Q values, but also consistently lower by a small amount. This is again attributed to the underestimated directivity in (4.21) associated with an infinitesimal dipole that was used in deriving the predicted Q.

In conclusion, an integral identity for the extinction cross section for an antenna over a dielectric half space has been derived and validated for a large and a small permittivity cases over a wide range of dipole position. An extinction cross section model based on a constant absorption efficiency with frequency-dependent directivity and impedance mismatch factor is effective in reproducing the integrand of the

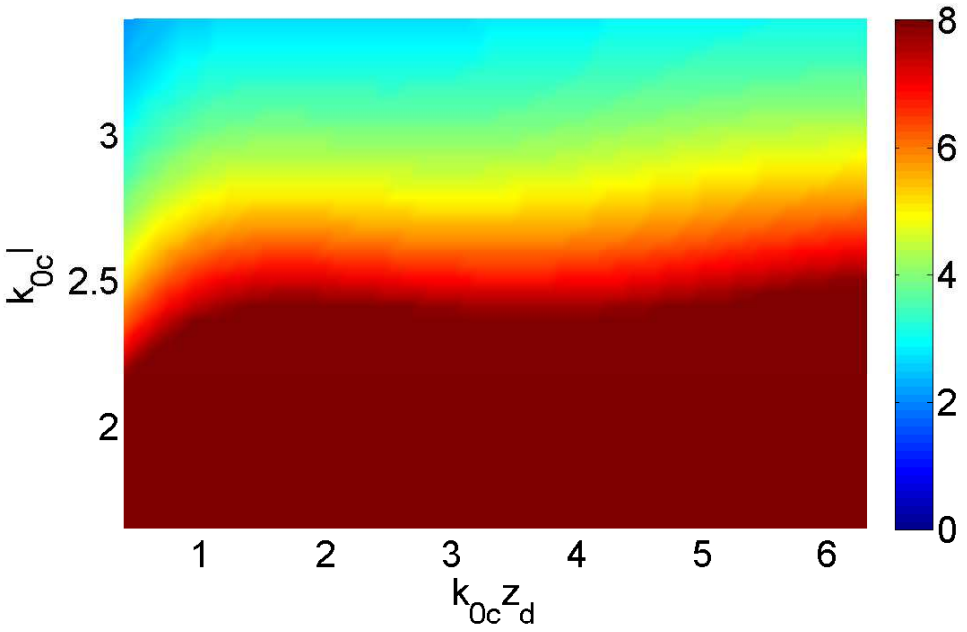

Figure 4.12. Surface plot for quality factor of a dipole above a dielectric half space when $\epsilon_r = 4$.

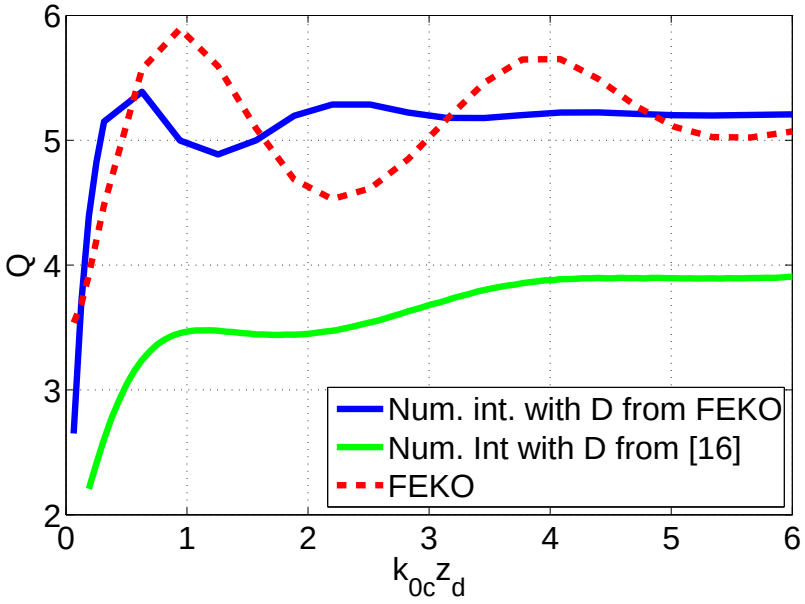

Figure 4.13. Quality factor comparison at $k_{0c}l = \pi$ when $\epsilon_r = 4$.

identity with a reasonable accuracy. The predicted resonance Q values were tested against simulated values and a reasonable agreement was found. It was found that the predicted Q values were consistently lower by a small amount than the simulated values due to the underestimated directivity associated with an infinitesimal dipole used in modeling the extinction cross section.

4.4.3 Effect of Permittivity on Q

A dipole of fixed electrical length $k_c l = \pi$ is placed above a dielectric half space, and its Q is studied as the permittivity is varied. A surface plot of the predicted Q is shown in Figure 4.14 as a function of permittivity and electrical separation. It is

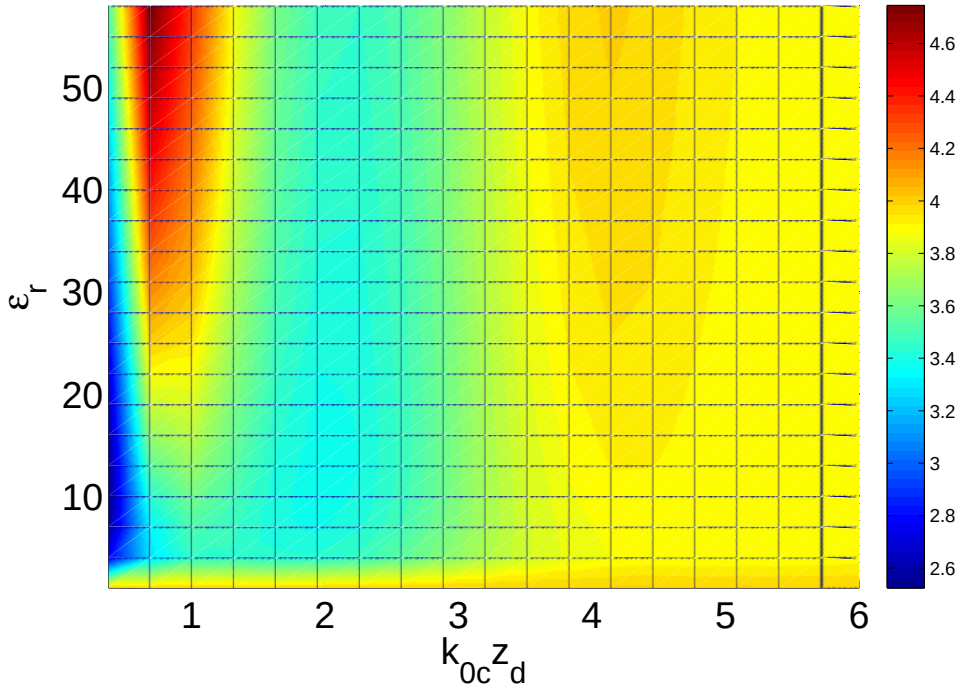

Figure 4.14. Quality factor for dipole of electrical length $k_{0c} l = \pi$ as function of permittivity ϵ_r.

noted that as the permittivity of the dielectric is reduced, the Q approaches a constant value of 4.4 associated with the antenna in an unbounded free spaces. In addition,

Q approaches the same constant value at large ground separation. Furthermore, it is noted that this Q associated with free space is not the minimum possible value. There are combinations of ϵ_r and $k_{0c}z_d$ that achieve lower Q values.

4.4.4 *Q* Comparison for a Small Antenna

In order to evaluate the effect of a half space for electrically small antenna above a dielectric half space, the Q value for a small antenna corresponding to $k_{0c}l = 1$ in free space is compared with the Q when it is placed above a dielectric half space. The free space Q is evaluated using (3.25), and it compared with the Q in the presence of a dielectric half space with $\epsilon_r = 40$ with respect to the electrical separation in Figure 4.15. At lower $k_{0c}z_d$, it is noted that the Q in the presence of a dielectric half space

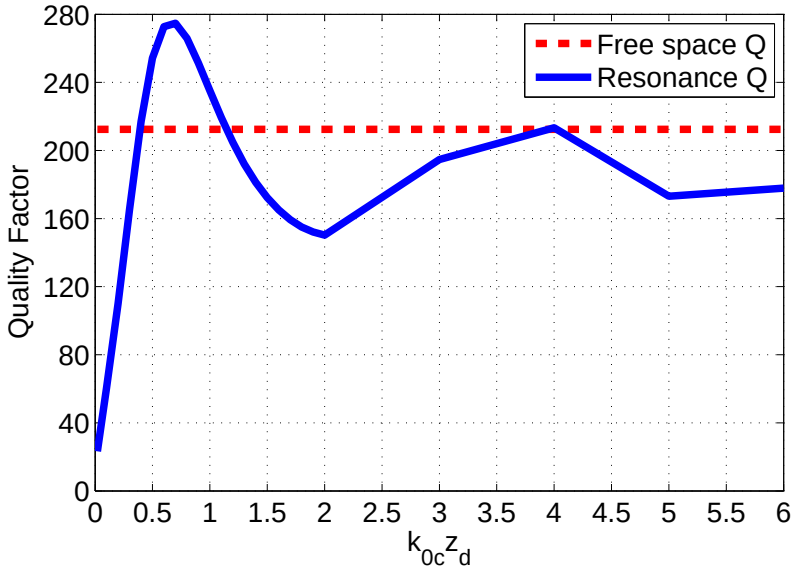

Figure 4.15. Comparison between the free space Q and the resonance Q of an electrically small antenna ($k_{0c}l = 1$) above a dielectric half space when $\epsilon_r = 40$.

is lower than free space Q, suggesting an increased bandwidth. As $k_{0c}z_d$ is increased, the Q of the dipole above a dielectric half space alternates around the Q of the same antenna in free space. With increasing separation to the material interface, a trend of converging Q toward the free space Q of the same antenna emerges.

CHAPTER 5

DIPOLE INSIDE A DIELECTRIC HALF SPACE

5.1 Approximate Integral Identity for Wire Dipole inside a Dielectric Half Space

In this section, we will study a dipole inside a dielectric half space for bandwidth. The problem configuration is illustrated in Figure 5.1.

The incident field is chosen to be normally incident on the free space-dielectric

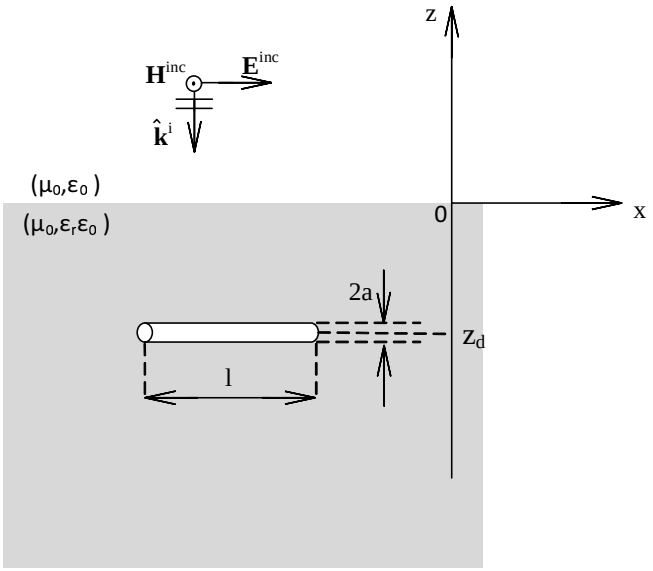

Figure 5.1. A thin wire dipole inside a dielectric half space.

interface from the free space side, so that the dipole will experience a single plane wave. An approximate integral identity for a dipole immersed in a dielectric half space can be obtained following the same process used for a dipole above a dielectric

half space in Chapter 4. in terms of the total fields on the antenna bounding surface S, the extinction cross section is given by

$$\sigma_{ext}(k) = \frac{\eta_0}{|E_0|^2}\mathrm{Re}\left\{\hat{x}E_0^* T^* \cdot (-\hat{z}) \times \oint_S \left[(\hat{n}\times\mathbf{H})\times(-\hat{z}) + \frac{1}{\eta}(\hat{n}\times\mathbf{E})\right] e^{-jkz'} ds'\right\}. \tag{5.1}$$

This is different from (4.7) in four aspects. First, the original source field is from the free space side, so the normalizing power density is $|E_0|^2/2\eta_0$. Second, the propagation direction of the incident wave the dipole experiences is the $-\hat{z}$ direction. Third, the wavenumber for the incident field is k. Finally, the transmission coefficient T is given by $T = 2\eta/(\eta+\eta_0)$. In the low frequency limit, σ_{ext} is expressed as

$$\begin{aligned}\sigma_{ext}(k) &= \frac{1}{|E_0|^2}\mathrm{Re}\left\{jk\frac{\eta_0}{\eta}E_0^* T^*\left(\hat{x}\cdot\frac{\mathbf{p}}{\epsilon_0} + \hat{y}\cdot\eta\mathbf{m}\right) + \mathcal{O}(k^2)\right\} \\ &= \mathrm{Re}\left\{jk\epsilon_r T^*\left(\hat{x}\cdot\frac{\mathbf{p}/\epsilon_0}{|E_0|} + \hat{y}\cdot\frac{\eta\mathbf{m}}{\eta_0|H_0|}\right) + \mathcal{O}(k^2)\right\}, \qquad k\to 0.\end{aligned} \tag{5.2}$$

Note that $E_0 = \eta_0 H_0$ because the antenna is illuminated from free space. A contour integral in the complex-k plane along the real-k axis as shown in Figure 2.3 gives an integral identity

$$\int_0^\infty \frac{\sigma_{ext}(k)}{k^2}dk = \frac{\pi\epsilon_r}{2}T\left(\hat{x}\cdot\frac{\mathbf{p}/\epsilon_0}{|E_0|} + \hat{y}\cdot\frac{\eta\mathbf{m}}{\eta_0|H_0|}\right). \tag{5.3}$$

The difference from (4.13) is that ϵ_r appears in the numerator. It should be remembered that the source field illuminates the medium interface from the free space side. The integral identity (5.3) is expected to be approximate because the forward scattering is not occurring in an unbounded space. In fact, the scattering configuration under consideration is closely related to the scattering by the same antenna in an unbounded dielectric space having the same relative permittivity as the dielectric half space. Similarly to dipole scattering above the free space-dielectric interface considered in Chapter 4, the integral sum rule (5.3) is expected to become

accurate when the induced static dipole moments **p** and **m** are not affected by the medium interface, i.e., when the dipole location is not close to the interface. It is necessary to validate (5.3) for the scattering configuration under consideration. For an example PEC thin-wire dipole of $l = 0.5$ m and $a = 2.5$ mm. Table 5.1 compares the two sides of the integral identity for different z-coordinate of the horizontal dipole z_d inside the dielectric. For all the depths considered, both sides agree within 4.1% or less, so the equality is validated for the test case. As in the case of a dipole over a dielectric half space, the difference between the two sides slightly increase when the dipole is placed close to the medium interface. The integral can be converted from one in terms of σ_{ext} to one involving σ_a using the relationship $\sigma_{ext} = \sigma_a/\eta_{abs}$. The absorption cross section is expressed as

$$\sigma_a = A_e(k) = \frac{\lambda_0^2}{4\pi} D(k)(1 - |\Gamma(k)|^2) = \frac{\pi}{k_0^2} D(k)(1 - |\Gamma(k)|^2). \tag{5.4}$$

In (5.4), the free space wavelength needs to be used because the far-zone direction of directivity evaluation is the direction of the source wave from free space. Once models for D and the impedance mismatch factor for a narrowband resonant antenna are developed and confirmed, the resonance Q can be predicted using (5.3).

5.2 Model for $1 - |\Gamma(k)|^2$

A similar reasoning applies to the mismatch of a dipole inside a dielectric half space as did for a dipole in free space above the medium interface. In other words, around the resonant wavenumber inside the dielectric k_c, the mismatch follows the standard 2nd-order resonance behavior. In the low frequency limit, the mismatch is of $\mathcal{O}(k^4)$. Hence, the same model given in (4.19) is adopted

$$(1 - |\Gamma(k)|^2) = \frac{k^2}{k_c^2((1 + (\frac{Q}{2})^2(\frac{k}{k_c} - \frac{k_c}{k})^2)}. \tag{5.5}$$

Table 5.1. Validaion of the integral identity for wire dipole inisde a dielectric half space for $\epsilon_r = 40$.

Position(z_d)	LHS	COMSOL($\frac{\mathbf{p}}{\epsilon_0}$)	RHS	Percent diff.
-0.01	0.0587	0.0131	0.0612	4.1
-0.02	0.0662	0.0142	0.0665	0.5
-0.03	0.0703	0.0154	0.0722	2.6
-0.04	0.0731	0.0161	0.0756	3.3
-0.05	0.0752	0.0164	0.0766	1.8
-0.06	0.0767	0.0169	0.0792	3.2
-0.10	0.0804	0.0177	0.0828	2.9
-0.125	0.0815	0.0179	0.0837	2.6
-0.15	0.0823	0.0179	0.0841	2.1
-0.20	0.0831	0.0181	0.0850	2.2
-0.25	0.0835	0.0183	0.0850	2.8
-0.30	0.0837	0.0183	0.0856	2.2
-0.35	0.0841	0.0183	0.0857	1.9
-0.40	0.0840	0.0183	0.0858	2.1
-0.45	0.0841	0.0184	0.0858	2.0
-0.50	0.0841	0.0184	0.0864	2.7
-1.0	0.0842	0.0184	0.0864	2.6

For an example, a dipole of $l = 0.5$ m and $a = 2.5$ mm, (5.5) was tested against FEKO simulation results for three different dipole locations $z_d = -0.05$ m, -0.5 m, and -0.85 m. Comparison between the modeled and simulated mismatches is made in Figure 5.2.

The model intends to capture the first, dominant resonance, so we conclude that (5.5) is adequate for modeling the mismatch. It can be noted that the resonance frequencies shifts to lower values compared with those of the same dipole above the half space. The frequency of the first resonance is 300MHz for the dipole above a half space and it is 47MHz when it is placed inside the dielectric which is scaled by $\sqrt{\epsilon_{ra}}$

5.3 Model for $D(k)$

As in the case of a dipole above a dielectric half space, the directivity expression from [17] is employed for a dipole inside a dielectric half space. The problem

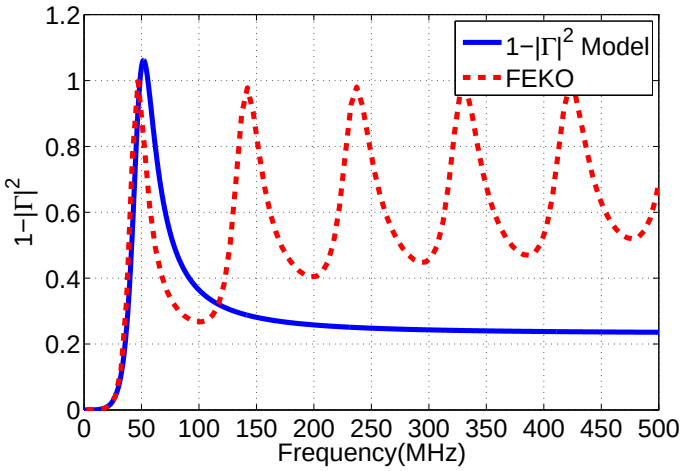

(a)

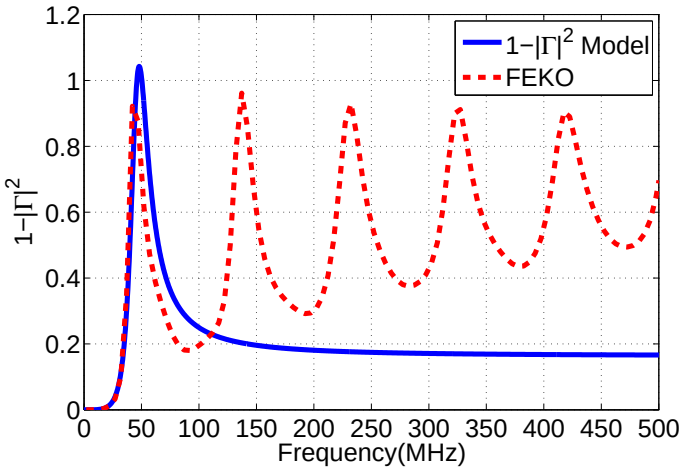

(b)

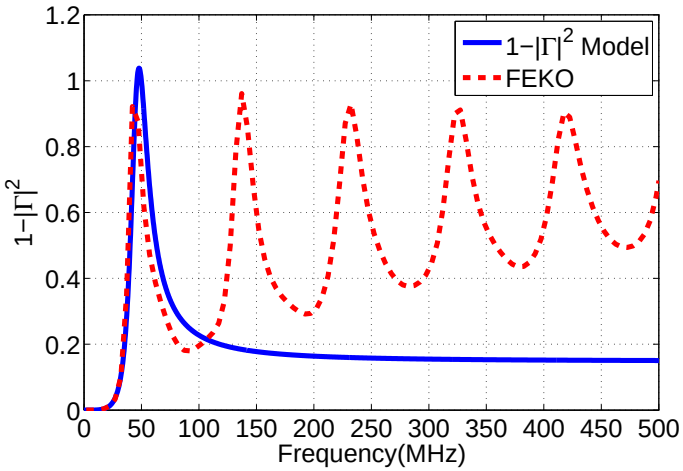

(c)

Figure 5.2. Comparison of $1 - |\Gamma(k)|^2$ at different distance z_d (a) $z_d = -0.05$ m. (b) $z_d = -0.5$ m. (c) $z_d = -0.85$ m.

is illustrated in Figure 5.3. It shows a Hertzian electric dipole inside a half space transmitting into free space.

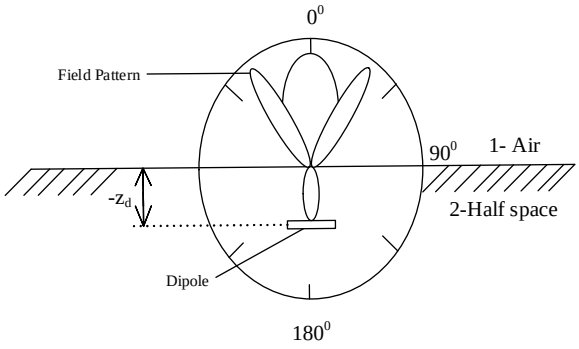

Figure 5.3. Smith's directive properties of a dipole antenna transmitting into air from half space

The directivity expression is [17]

$$D_e = \frac{8k_{21}}{(1+k_{12})^2}\left\{\frac{4}{3} - \frac{1}{k_1}\int_0^{k_{21}} \gamma_1 \cdot \left[R_{\parallel} - \left(\frac{k_1}{\gamma_1}\right)^2 R_{\perp}\right] \cdot \cos\left(2\gamma_1 h\right)\rho d\rho \right. \\ \left. -\frac{1}{k_1}\int_{k_{21}}^{1} \gamma_1 \left[\mathrm{Re}(R_{\parallel} e^{-2\gamma_1 h}) + \left(\frac{k_1}{\gamma_1}\right)^2 \mathrm{Re}(R_{\perp} e^{-2|\gamma_1| h})\right] \rho d\rho \right\}^{-1}. \tag{5.6}$$

where $k_{12} = k_1/k_2$, $k_{21} = k_2/k_1$, the parallel reflection coefficient $R_{\parallel}(K) = (k_2^2\gamma_1 - k_1^2\gamma_2)/(k_2^2\gamma_1 + k_1^2\gamma_2)$, the perpendicular reflection coefficient $R_{\perp}(K) = (\gamma_1 - \gamma_2)/(\gamma_1 + \gamma_2)$, the parallel transmission coefficient $T_{\parallel}(K) = 2k_1k_2\gamma_1/(k_2^2\gamma_1 + k_1^2\gamma_2)$, $T_{\perp} = 2\gamma_1(\gamma_1 + \gamma_2)$, $\gamma_1 = -\jmath\sqrt{K^2 - k_1^2}$, $\gamma_2 = -\jmath\sqrt{K^2 - k_2^2}$, $\rho = K/k_1$, and $K = \sqrt{k_x^2 + k_y^2}$. As a validation of the theoretical formulation as well as its numerical implementation, the directivity in the $+z$ axis direction computed from (5.6) and obtained from FEKO simulation of a very short dipole ($l = 0.01\lambda$) are compared in Figure 5.4 at two different dipole locations. An excellent agreement is observed. Since our model of D will use the directivity of an infinitesimal dipole and it will be used in deriving the resonance Q bound of dipoles of non-negligible lengths, it is worthwhile

to compare the model to the simulated directivity for a dipole (a half wavelength inside the dielectric at 47 MHz). It can be observed that the model is accurate in the low frequency range only as shown in Figure (5.5). Still, the directivity of (5.6) shows a reasonable agreement around the resonance frequency of 47 MHz. Together with the fact that $\sigma_{ext}(k)$ in (5.3) is weighted by $\frac{1}{k^2}$, inaccuracy of D at high frequencies does not significantly compromise the accuracy of the resulting Q bound.

5.4 Numerical Result

5.4.1 High permittivity case $\epsilon_r = 40$

For a high permittivity test case, $\epsilon_r = 40$ is chosen. The accuracy of the extinction cross section and the resultant integrand of (5.3) between the model and numerical simulation is first checked to validate the model for σ_{ext}. For an example, a case with $l = 0.5$ m, $a = 2.55$ mm and $z_d = -0.5$ m the integrand of (5.3) computed in three different methods are compared in Figure 5.6. Figure 5.7 shows that the two integrands generated using two different directitivity values and together with the mismatch models (5.5) closely follow the FEKO-generated integrand. Some of this difference between the modeled quantities (solid blue) and the numerical analysis results (red dash) is attributed to the directivity of an infinitesimal dipole used for D. If the exact, numerically obtained directivity is used instead, the agreement of σ_{ext} between the model (solid green) and the simulation results (red dash) slightly improves.

Over a range of the dipoles electrical length, $k_c l$, and the electrical location of the antenna in z, $k_c z_d$, the predicted resonance Q value is shown as a color plot in the Figure 5.8. A horizontal cut in Figure 5.8 at $k_c l = \pi$ corresponds to a half-wavelength dipole inside the dielectric. The predicted Q values and those from numerical simulations are compared Figure 5.9. In most of the $k_c z_d$ range, the theory slightly

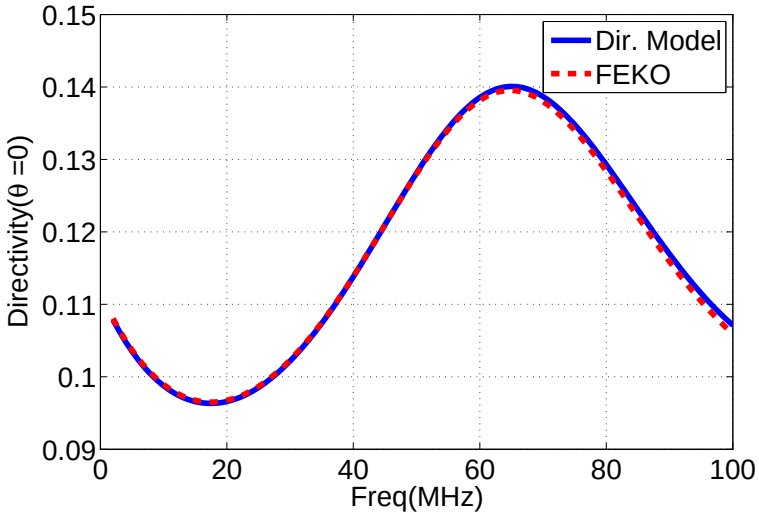

(a)

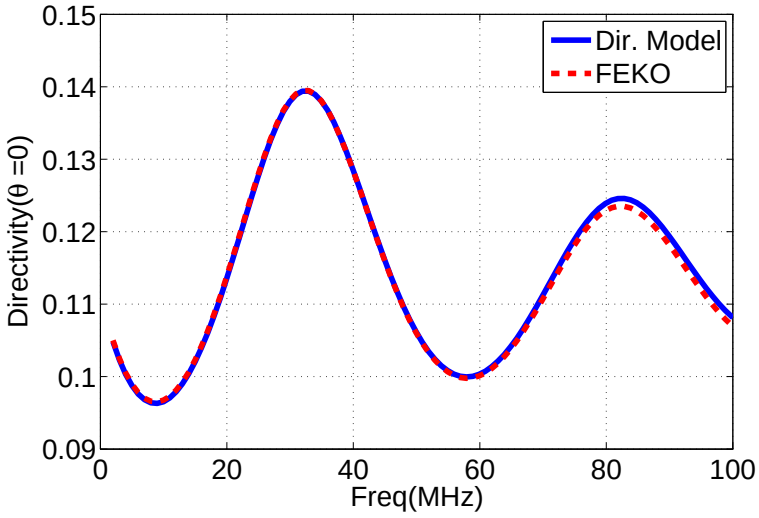

(b)

Figure 5.4. Comparison between directivity from FEKO and [17] at (a) $z_d = -0.25$ m. (b) $z_d = -0.5$ m.

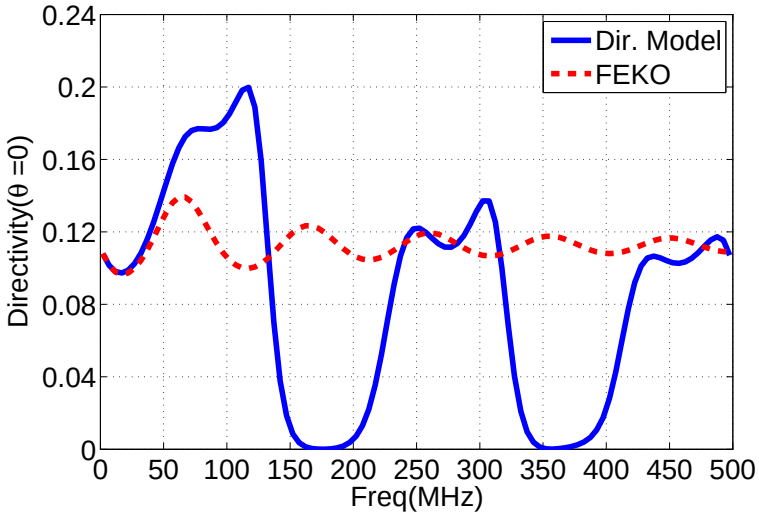

(a)

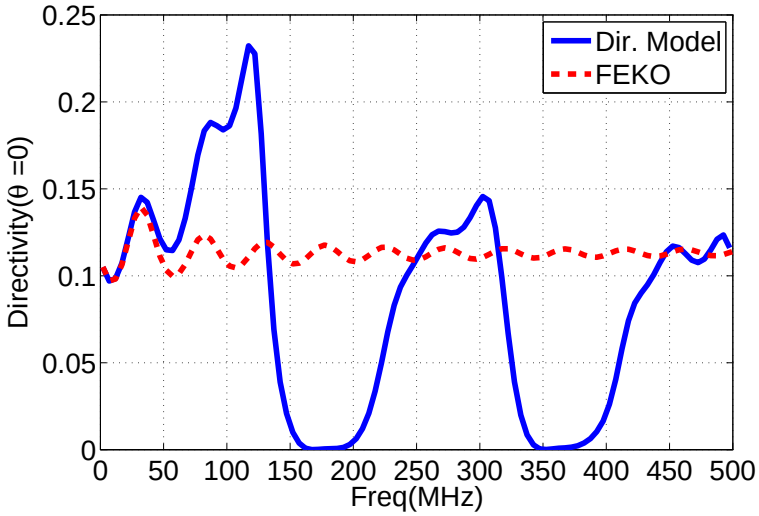

(b)

Figure 5.5. Comparison between directivity from FEKO and [17] at (a) $z_d = -0.25$ m. (b) $z_d = -0.5$ m.

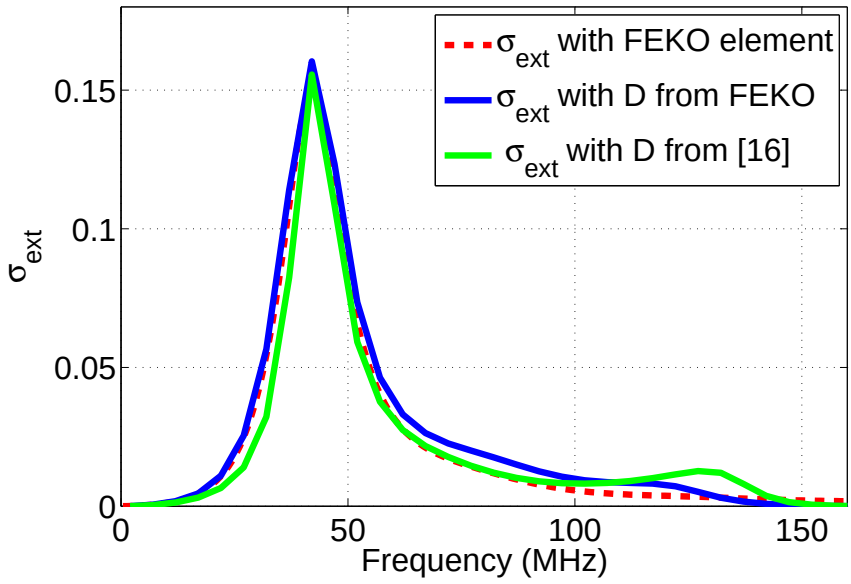

Figure 5.6. Comparison between σ_{ext} from FEKO receiving antenna, σ_{ext} using directivity from (5.6) and σ_{ext} using directivity from FEKO at $z_d = -0.5$ m.

underestimates the resonance Q, which is in part attributed to the slightly lower value of the directivity D used in the model.

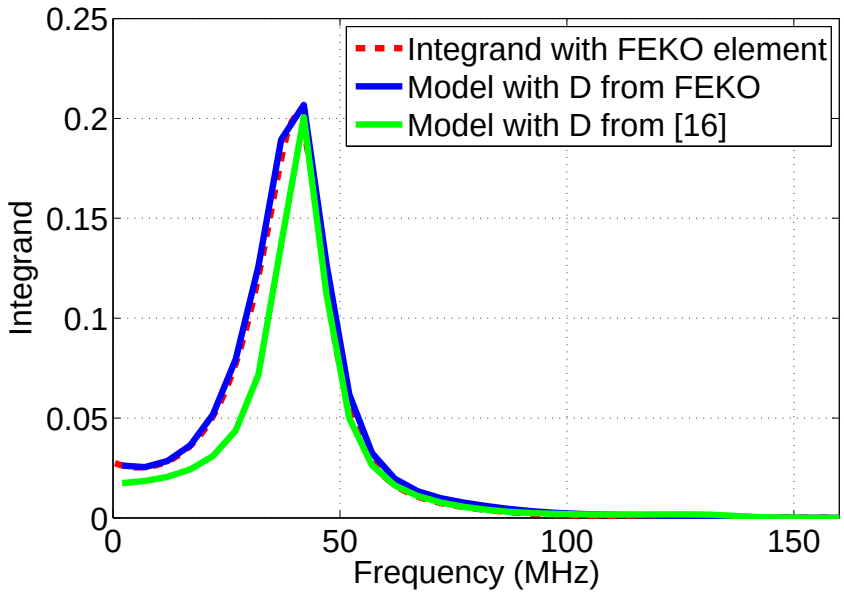

Figure 5.7. Comparison between integrand from FEKO receiving antenna, one using directivity from (5.6), and one using directivity from FEKO at $z_d = -0.5$ m.

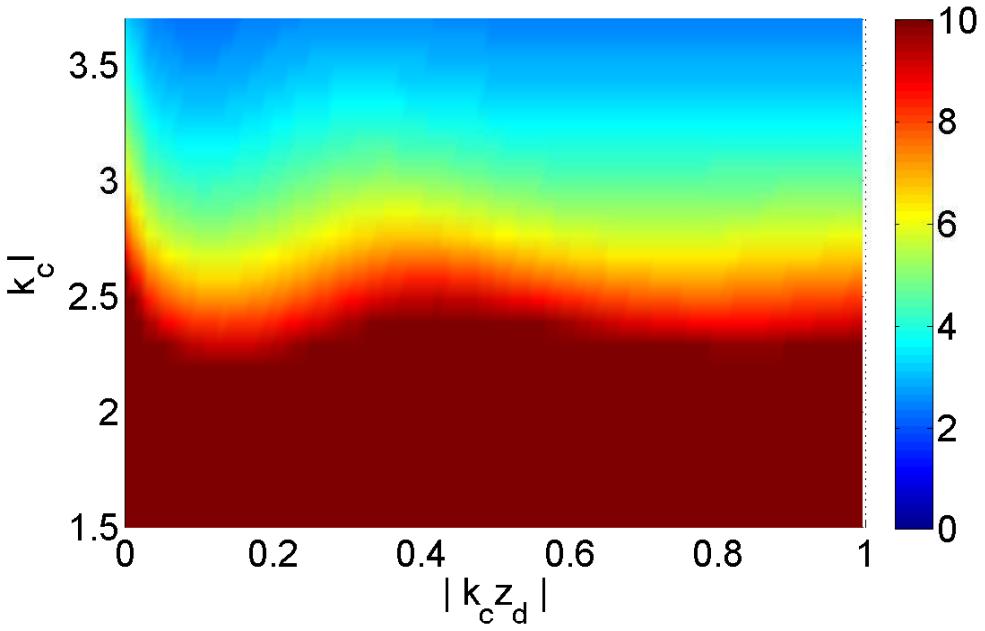

Figure 5.8. Surface plot for quality factor for dipole inside a dielectric half space when $\epsilon_r = 40$.

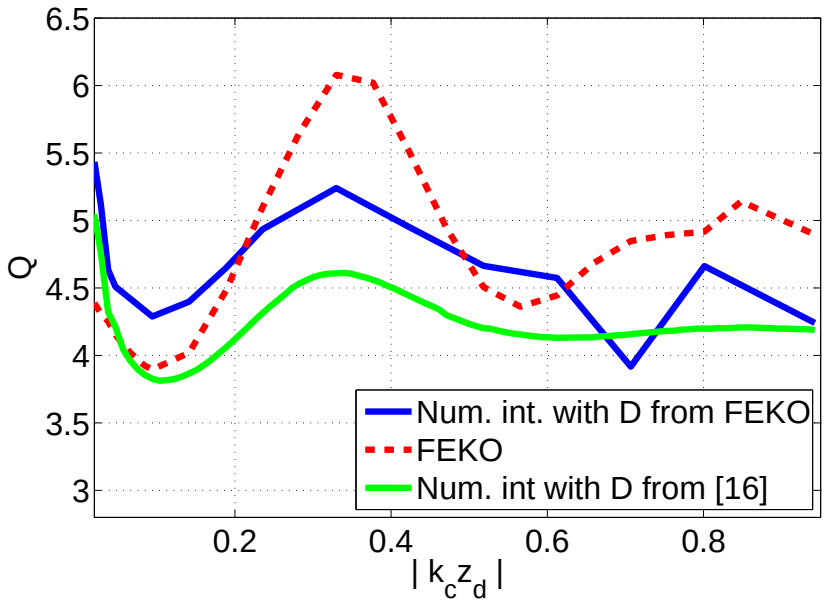

Figure 5.9. Quality factor comparison at $k_c l = \pi$ when $\epsilon_r = 40$

5.4.2 Low permittivity case $\epsilon_r = 4$

The derived integral identity is first tested for this case. For the thin-wire dipole with $l = 0.5$ m, $a = 2.5$ mm, both sides of the integral identity (5.3) are compared in Table 5.2. A reasonable agreement with a maximum difference of 5.8% is observed, thus validating the approximate identity.

A surface plot is plotted in Figure 5.10 for the predicted Q as a function of the electrical length and the position along the z axis inside the dielectric. For any fixed electrical length, the Q is a function of the dipole position relative to the medium interface. Inside this low permittivity dielectric, Q depends more weakly on $k_c z_d$ than in the high permittivity dielectric case. In Figure 5.11, the predicted Q is compared with the actual Q from FEKO analysis for the half-wave dipole case. In most of the range considered, the predicted Q is slightly lower than the actual Q obtained from FEKO simulations, part of which is attributed to the directivity of an infinitesimal dipole used in constructing the model of σ_{ext}. In conclusion, an approximate integral

Table 5.2. Validation of integral identity for a wire dipole inside dielectric half space for $\epsilon_r = 4$.

Position(z_d)	LHS	COMSOL($\frac{\mathrm{P}}{\epsilon_0}$)	RHS	Percent diff.
-0.01	0.0386	0.0144	0.0403	4.2
-0.02	0.0417	0.0156	0.0435	4.1
-0.03	0.0435	0.0160	0.0447	2.7
-0.04	0.0447	0.0170	0.0460	2.8
-0.05	0.0456	0.0170	0.0464	1.7
-0.06	0.0463	0.0173	0.0484	5.8
-0.10	0.0479	0.0180	0.0502	4.6
-0.15	0.0486	0.0182	0.0509	4.5
-0.20	0.0480	0.0185	0.0512	6.3
-0.25	0.0492	0.0185	0.0514	4.3
-0.30	0.0492	0.0185	0.0514	4.3
-0.35	0.0492	0.0185	0.0515	4.7
-0.40	0.0492	0.0185	0.0515	4.7
-0.45	0.0492	0.0185	0.0516	4.7
-0.50	0.0491	0.0185	0.0516	4.8
-1.0	0.0493	0.0185	0.0516	4.5

identity for the extinction cross section of a dipole antenna inside a dielectric half space was derived and numerically validated. Using a model for the extinction cross section for a narrowband dipole, the resonance Q value was predicted as a function of the antenna length and position relative to the free space-dielectric interface. For two example media having a high and low permittivities, the predicted Q values were compared with the actual Q values obtained from simulations and a reasonable agreement was observed.

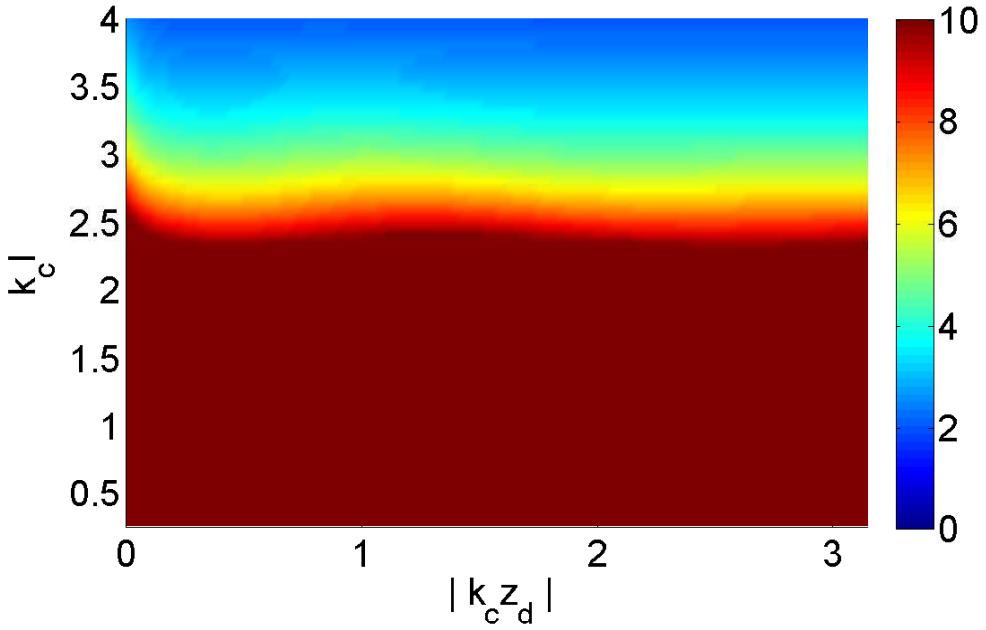

Figure 5.10. Surface plot for quality factor for dipole inside a dielectric half space $\epsilon_r = 4$.

5.4.3 Effect of Permittivity on Q

In this section, quality factor Q of a thin wire dipole inside a dielectric as a function of permittivity of the half space is studied. The thin wire dipole has a fixed of physical length ($l = 0.5$ m). In 5.12, the predicted Q is plotted as a function of the relative permittivity and the electrical position($|k_c z_d|$) inside the dielectric. At high

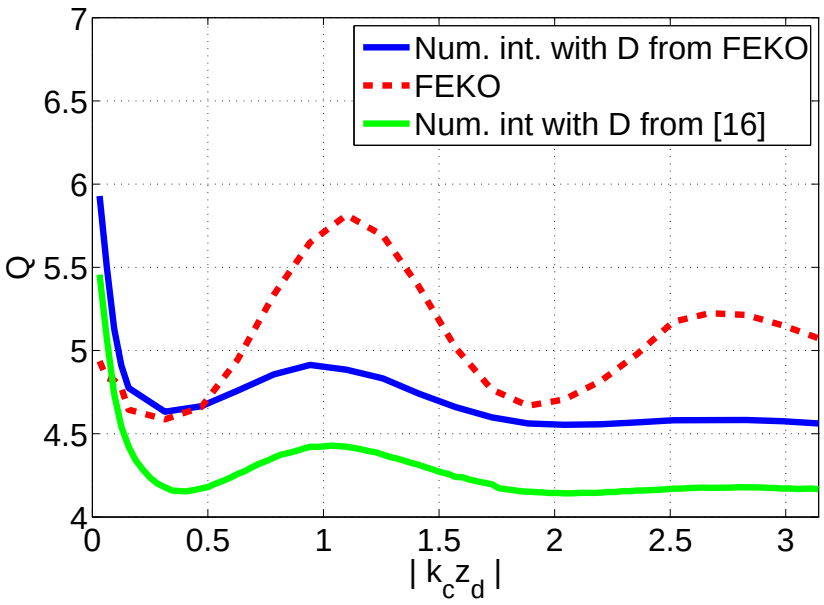

Figure 5.11. Quality factor comparison at $k_c l = \pi$ using directitiy from FEKO.

values of permittivity, predicited Q shows a larger variation with respect to antenna position compared with low permittivity cases. The predicited Q cases approaches a constant value associated with the antenna in unbounded free space as ϵ_r is reduced toward unity. Also, at large electrical separations from the interface, the predicited Q approaches approaches another constant associated with the same antenna in an unbounded dielectric medium.

5.4.4 *Q* Comparison for a Small Antenna

In order to evaluate the effect of an interface with free space for an electrically small antenna inside a dielectric half space, the Q value for a small dipole of $k_c l = 1$ in unbounded dielectric is compared with the Q of the same antenna is inside a dielectric half space. The antenna Q in an unbounded dielectric is evaluated using (3.25) with the impedance and wavenumber evaluated for dielectric medium. This is compared with Q of the same dipole when the dielectric becomes a half space in Figure 4.15 with respect to the electrical separation to the free space-dielectric interface.

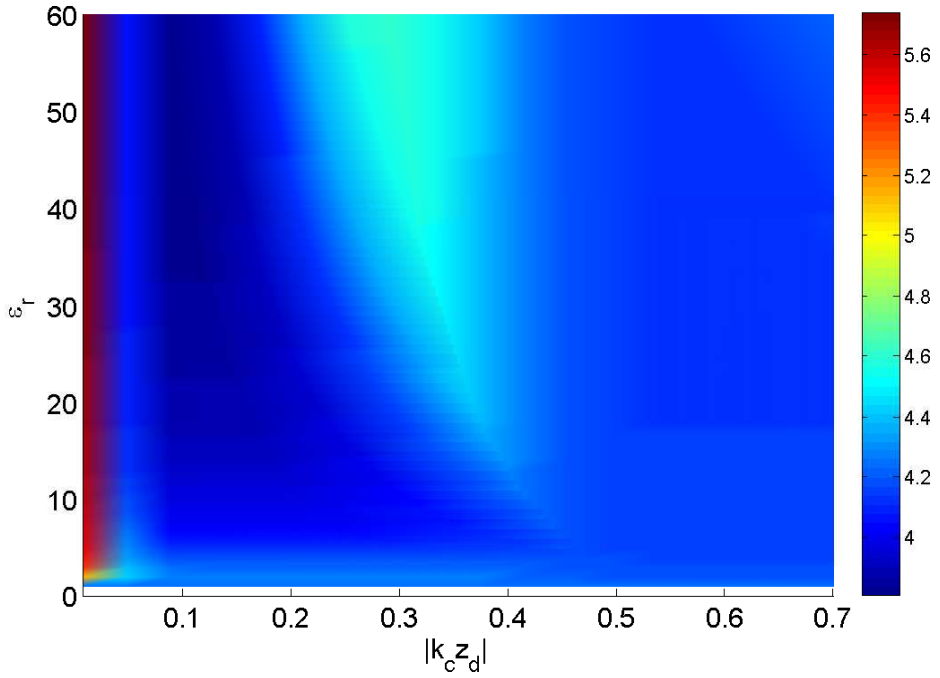

Figure 5.12. Quality factor for a dipole fixed length 0.5λ as function of permittivity ϵ_r.

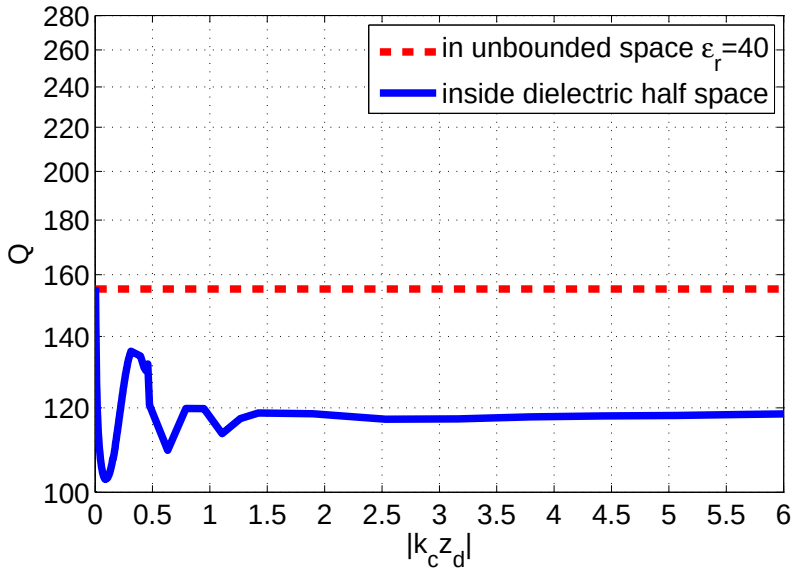

Figure 5.13. Comparison of free-space Q and resonance Q of an electrically small antenna ($k_c l = 1$) inside a dielectric half space of $\epsilon_r = 40$.

CHAPTER 6

CONCLUSION

The resonance quality factor Q of a thin wire dipole in the presence of a conducting ground plane has been studied. An integral sum rule for the extinction cross section of the antenna was first derived. For narrowband resonance response, a mathematical model for the impedance mismatch factor was developed. The directivity of an infinitesimal horizontal dipole over a ground was used together with the mismatch factor in the integral sum rule to derive the Q bound. A closed-form expression for the antenna Q was obtained as a function of ground separation separation and electrostatic polarizability of the antenna. With respect to the ground separation, the predicted lowest quality factor which correspond to the broadest bandwidth was confirmed using full-wave numerical analysis. For dipole antennas backed by a ground plane quater-wave separation is typically chosen, but the highest bandwidth or lowest quality factor was obtained at a distance approximately $\lambda/3$. At electrically large ground separation, the Q approaches a constant value. This is expected because the effect of the ground plane is minimal when an antenna is far separated from the ground, approaching the free space characteristics. However, when the antenna is close to the ground plane, the quality factor increases.

In the second part, a dipole in the presence of a dielectric half space was studied. Both a dipole above a dielectric half space as well as a dipole inside a dielectric half space were considered. An integral identity for the extinction cross section was derived, and numerically validated using an example configuration for each case. For a high and a low relative permittivities of 40 and 4, the predicted Q bound was evalu-

ated as a function of the antenna position and the electrical length of the dipole. For resonant half wave dipoles, the predicted Q values were compared with full-wave numerical simulation results, which showed a reasonable agreement. For larger electrical separations between the medium interface and the wire dipole, the Q was predicted to approach constant value as expected. When a resonant antenna is not in free space, the quality factor and the associated impedance bandwidth are different from those of the same antenna in free space. To date, the standard approach to evaluating the antenna Q and bandwidth for antennas in simple, non-free space environments such as a ground plane or material half space has been frequency-swept, full-wave numerical simulation. The Q bounds in this study represent one of the first efforts to evaluate and predict the antenna characteristics in practical operating environments without resorting to numerical analysis.

APPENDIX A

PROOF OF QUALITY FACTOR'S LIMIT

In this section, details of the integral evaluation are provided for (3.23), which is reproduced below.

$$\int_0^\infty \frac{dk}{k^2(1+(\frac{Q}{2})^2(\frac{k}{k_c}-\frac{k_c}{k})^2)} \leq \frac{R(k_c d)k_c^2\eta_{abs}}{2}(\bar{e_t}^*.\gamma_{be}.\hat{e}^i) \tag{A.1}$$

Here k is the free space wavenumber, k_c is the wave-number at the resonant frequency of the antenna, Q is the resonance quality factor, η_{abs} is the absorption efficiency and γ_{be} is the polarizability of the antenna. An indefinite integral of the form

$$\int_0^\infty \frac{dk}{R_2} \tag{A.2}$$

is available in [19], where R_2 is a polynomial in k of the fourth order. The LHS of (A.1) can rewritten as

$$\frac{1}{k_c}\int_0^\infty \frac{dx}{\frac{Q^2x^4}{4}+\left[1-\frac{Q^2}{2}\right]x^2+\frac{Q^2}{4}} \tag{A.3}$$

where x= $\frac{k}{k_c}$ and $dx = \frac{dk}{dk_c}$. The function $R_k = a + bx^2 + cx^4$ can be equated to the denominator of (A.3), giving $a = \frac{Q^2}{4}$, $b = \left[1-\frac{Q^2}{2}\right]$ and $c = \frac{Q^2}{4}$. A condition to check according to [19] is if $h^2 < 0$. (A.2) has a closed-form result given by

$$\int_0^\infty \frac{dk}{R_2} = \frac{1}{4cq^3\sin\alpha}\left\{\frac{\sin\alpha}{2}\ln\left[\frac{x^2+2qx\cos\frac{\alpha}{2}+q^2}{x^2-2qx\cos\frac{\alpha}{2}+q^2}\right]+2\cos\frac{\alpha}{2}\tan^{-1}\left[\frac{x^2-q^2}{2qx\sin\frac{\alpha}{2}}\right]\right\}\Big|_0^\infty \tag{A.4}$$

where $h = \sqrt{b^2 - 4ac}$. After substituting a,b and into h, we find $h^2 = 1 - Q^2$. Since $Q > 1$ for practical narrowband antennas, it is concluded that the condition $h^2 < 0$ is satisfied. In (A.4), $q = \sqrt[4]{\frac{a}{c}} = 1$, $\cos\alpha = \left[1 - \frac{2}{Q^2}\right]$, $\sin\frac{\alpha}{2} = \frac{1}{Q}$ and $\sin\alpha = \frac{2(\sqrt{Q^2-1})}{Q^2}$. After substituting these into (A.4), the first term in the braces is zero because $ln(1) = 0$ at both limits. The second term in the braces and the factor $\frac{1}{4cq^3\sin\alpha}$ give a simple answer

$$\int_0^\infty \frac{dk}{R_2} = \frac{1}{2k_c(\sqrt{Q^2-1})}\left\{0 + \frac{2(\sqrt{Q^2-1})}{Q}\left[\frac{\pi}{2} - (-\frac{\pi}{2})\right]\right\} = \frac{1}{k_c}\frac{\pi}{Q} \tag{A.5}$$

Hence, (A.1) becomes

$$\frac{1}{k_c}\frac{\pi}{Q} \leq \frac{R(k_c d)k_c^2\eta_{abs}}{2}(\bar{e_t}^*.\gamma_{be}.\hat{e}^i) \tag{A.6}$$

The final expression for the Q bound is

$$Q \geq \frac{\lambda_c^3}{R(k_c d)4\pi^2\eta_{abs}(\bar{e_t}^*.\gamma_{be}.\hat{e}^i)} \tag{A.7}$$

which is given as (3.24)

APPENDIX B

NUMERICAL EVALUATION OF POLARIZABILITIES

Static polarizability values used in all cases in this study were evaluated numerically using COMSOL Multiphysics, which is based on the finite-element technique. Electrostatic and magnetostatic dipole moments $\mathbf{p}$ and $\mathbf{m}$ of a scatterer are defined by [12]

$$\mathbf{p}/\epsilon_0 = \oint_S \left(\hat{n}\Phi_0 - \mathbf{r}' \frac{\partial \Phi_0}{\partial n} \right) ds', \text{ and } \eta_0 \mathbf{m} = \oint_S \left(\hat{n}\Psi_0 - \mathbf{r}' \frac{\partial \Psi_0}{\partial n} \right) ds'. \tag{B.1}$$

where ϵ_0 is the permittivity of free space, S is the surface that encloses the antenna, Φ_0 is the electrostatic potential, Ψ_0 is the magnetostatic potential, $\mathbf{r}'$ is the position vector of the antenna, and η_0 is the free space intrinsic impedance. For the thin-wire dipole antenna considered in this study, the magnetostatic polarizability is minimal and it can be set to zero because dipole antenna is perfectly conducting.

In COMSOL Multiphysics natively supports the surface integral for, $\mathbf{p}/\epsilon_0$ is evaluated on a closed surface of the dipole. For the rhs of the integral to represent the polarizability value, the strength of the background static field should by set to unity. This can be achieved by applying an appropriate electric potential difference for giving a unit field $E^{inc} = \hat{x}V/m = 1$ onto the antennas as shown in Figure B.1.

The electric potential at $x = -l_x/2$ is set to $V = -l_x/2$ and $V = l_x/2$ at $x = -l_x/2$. Then $\mathbf{E}^{inc} = \hat{x}(\frac{l_x}{2} - \frac{-l_x}{2})/l_x = \hat{x}V/m$. A unknown, constant potential is assigned to the antenna surface, as appropriate for PEC material. Both the box

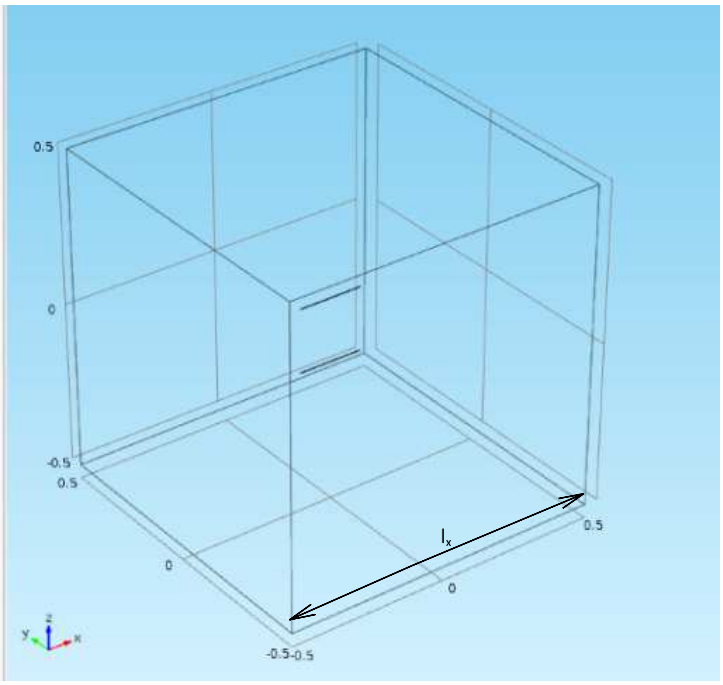

Figure B.1. Model in COMSOL

and the dipole are then finely meshed. The electric polarizability is evaluated as a superposition of contributions from each discretized element surface of S as

$$\mathbf{p}/\epsilon_0 = \frac{1}{\epsilon_0} \sum_{i=1}^{N} \left(\sum_{j=1}^{M} \mathbf{p}_j \right) \tag{B.2}$$

where $\mathbf{p}_j$ is the polarizability contribution from each tetrahedral on the dipole surface S, N is the number of the faces and M is the number of tetrahedral on each face of the dipole. A large value of M is associated with a very fine mesh and thus gives a numerically converged value of the electrostatic polarizability.

BIBLIOGRAPHY

[1] L. J. Chu, "Physical limitation of omni-directional antenna," *Journal of Applied Physics*, vol. 19, pp. 1163–1175, Dec. 1948.

[2] J. S. McLean, "A re-examiniation of the fundamental limits on the radiation of Q of electrically small antennas," *IEEE Transanctions on Antennas and Propagation Magazine*, vol. 44, no. 5, pp. 672–676, May 1996.

[3] M. Gustafsson, C. Sohl, and G. Kristensson, "Illustrations of new physical bounds on linearly polarized antennas," *IEEE Transanctions on Antennas and Propagation*, vol. 57, no. 5, pp. 1679–1686, May. 2009.

[4] H. A. Wheeler, "Fundamental limitation of small antennas," *Proceedings of I.R.E*, vol. 35, no. 5, pp. 1479–1484, Dec. 1947.

[5] R. E. Collin and S. Rothschild, "Evaluation of antenna Q," *IEEE Transanctions on Antennas and Propagation*, vol. 12, no. 1, pp. 23–27, Jan. 1964.

[6] R. L. Fante, "Quality factor of general antennas," *IEEE Transanctions on Antennas and Propagation*, vol. AP-17, no. 1, pp. 151–155, Mar. 1969.

[7] H. L. Thal, "New radiation Q limits for sperical wire antennas," *IEEE Transanctions on Antennas and Propagation*, no. 10, pp. 2757–2763, Oct. 2006.

[8] R. C. Hansen and R. E. Collin, "A new Chu formula for Q," *IEEE Antennas and Propagation Magazine*, vol. 51, no. 5, pp. 38–41, Oct. 2009.

[9] J. C. Sten, A. Hujanen, and P. K. Koivisto, "Quality factor of an electrically small antenna radiating close to a conducting plane," *IEEE Transanctions on Antennas and Propagation*, vol. 49, no. 5, pp. 829–835, May. 2001.

[10] H. Chang, Y. H. Cho, and D.-H. Kwon, "Radiation Q bounds for small electric dipoles over a conducting ground plane," *IEEE Transanctions on Antennas and Propagation*, vol. 62, no. 4, pp. 2031–2040, Apr. 2014.

[11] M. Gustafsson, C. Sohl, and G. Kristensson, "Physical limitation on antennas of arbitrary shape," *Proceedings of the Royal Society A*, vol. 10, no. 10, pp. 2589–2607, Jul. 2007.

[12] R. E. Kleinman, *Low and High Frequency Asymptotics*. North-Holland: Elserveir Science Publishers, 1986.

[13] C. A. Balanis, *Antenna Theory: Analysis and Design*, 3rd ed. New York, NY: Wiley, 2005.

[14] D.-H. Kwon, "Sum rule for conductor-backed wire-dipole," *Proceedings of the IEEE Antennas and Propagation Society International Symposium*, pp. 1–2, Jul. 2012.

[15] D. M. Pozar, *Microwave Engineering*, 4th ed. Hoboken, NJ: John Wiley and Sons Inc., 2012.

[16] J. C. Lin, *Advances in Electromagnetic Fields in Living Systems*. New York, Ph: Springer Science and Business Media Inc, 2005.

[17] G. S. Smith, "Directive properties of antennas for transmission into a material half-space," *IEEE Transactions on Antennas and Propagation*, vol. AP-32, no. 3, pp. 232–246, Mar. 1984.

[18] D. B. Rutledge and M. S. Muha, "Imaging antenna array," *IEEE Transactions on Antennas and Propagation*, vol. AP-30, no. 4, pp. 535–540, Jul. 1982.

[19] I. S. Gradshteyn and I. M. Ryzhik, *Table of Integrals Series and Products*, 4th ed. Waltham, MA: Academic Press, 2000.